

ETD Archive

2018

Effect of History on the Binary Adsorption Equilibria of Aluminium Terephthalate (Mil-53(Al))

Ufuoma Israel Kara
Cleveland State University

Follow this and additional works at: <https://engagedscholarship.csuohio.edu/etdarchive>

 Part of the [Chemical Engineering Commons](#)

[How does access to this work benefit you? Let us know!](#)

Recommended Citation

Kara, Ufuoma Israel, "Effect of History on the Binary Adsorption Equilibria of Aluminium Terephthalate (Mil-53(Al))" (2018). *ETD Archive*. 1077.

<https://engagedscholarship.csuohio.edu/etdarchive/1077>

This Thesis is brought to you for free and open access by EngagedScholarship@CSU. It has been accepted for inclusion in ETD Archive by an authorized administrator of EngagedScholarship@CSU. For more information, please contact library.es@csuohio.edu.

EFFECT OF HISTORY ON THE BINARY ADSORPTION EQUILIBRIA OF
ALUMINIUM TEREPHTHALATE (MIL-53(AI))

UFUOMA I. KARA

Bachelor of Engineering in Chemical Engineering

University of Benin

April 2014

submitted in partial fulfillment of the requirements for the degree

MASTER OF SCIENCE IN CHEMICAL ENGINEERING

at

CLEVELAND STATE UNIVERSITY

AUGUST 2018

We hereby approve this thesis

for

UFUOMA KARA

Candidate for the Master of Science in Chemical Engineering degree for the

Department of Chemical and Biomedical Engineering

and

CLEVELAND STATE UNIVERSITY'S

College of Graduate Studies

Thesis Chairperson, Sasidhar Gumma, Ph.D.

Department of Chemical & Biomedical Engineering
Department & Date

Thesis Committee Member, Jorge E. Gatica, Ph.D.

Department of Chemical & Biomedical Engineering
Department & Date

Thesis Committee Member, Christopher L. Wirth, Ph.D.

Department of Chemical & Biomedical Engineering
Department & Date

Student's Date of Defense: July 23, 2018

ACKNOWLEDGEMENT

My sincere gratitude goes to God for the privilege of studying for a Master's degree here in the United States. I am also very thankful to my parents and siblings, whose selfless sacrifices, unfailing love, and relentless encouragement laid the foundation and paved the way for me to pursue the dream of earning a Master's degree. Their continuous moral support made it possible for me to complete this program. I am forever grateful and indebted to them.

I am very thankful to my Advisor, Dr. Sasidhar Gumma for his patience, kindness, and support during the period of my studies. His guidance helped me improve on my research and writing skills. I am also very appreciative of Dr. Jorge Gatica and Christopher Wirth, for their tutelage during my academic program and their willingness to serve as members of my Thesis Committee. Also, thank you to members of my research group for their assistance in different ways. I am grateful to Dr. Orhan Talu for his tutelage and the unfettered access he granted me into his laboratory as well.

I am especially thankful to Ms. Rebecca Laird and Darlene Montgomery for their kindheartedness, guidance and support. I am extremely thankful to the Department of Chemical Engineering and Biomedical Engineering for the opportunity to serve as a graduate assistant and the financial support it provided. Lastly, I will like to appreciate my girlfriend Areeveso Precious for her unrelenting support and encouragement during the period of my study.

EFFECT OF HISTORY ON THE BINARY ADSORPTION EQUILIBRIA OF
ALUMINIUM TEREPHTHALATE (MIL-53(Al))

UFUOMA KARA

ABSTRACT

Metal organic frameworks (MOFs) are highly porous solids with potential applications in a wide range of fields including gas separations and catalysis. Most of porous solids used in these applications such as zeolites and activated carbon usually have rigid structures. In contrast, a number of metal-organic frameworks (MOFs) exhibit structural transformation in response to external stimuli. Such materials show promise for applications such as sensors, actuators and adsorptive separations. Several thermodynamic formalisms were proposed in literature to explain this phenomenon, often known as “gate-opening” or “breathing” of the MOF material.

In this study, the adsorptive behavior of MIL-53(Al), a MOF that undergoes a change in volume of about 40% when transiting between its narrow pore (np) and large pore (lp) phases was measured. The binary adsorption characteristics of this MOF depend on its history, which makes these experimental measurements and its modeling more complicated. In literature, mixed gas adsorption equilibrium data on this material is limited to CO₂/CH₄ mixtures. Moreover, available models in literature cannot describe the history dependence of equilibrium data for gas mixtures.

The pure component adsorption equilibria at 293 K on the narrow pore phase showed a significantly higher capacity for CO₂ (compared to that of N₂) in the sub-atmospheric pressure region. In addition, the binary adsorption equilibria results showed that the narrow pore phase exhibited a high CO₂/N₂ selectivity, while the selectivity was

close to unity on the large pore phase.

The pure component isotherms on this material were modeled using a Langmuir type isotherm for each phase that includes a pore opening parameter dependent on spreading pressure (SPDPLM Model), as proposed in literature. In addition, for the first time in this work the SPDPLM was readily extended to binary mixtures, without any additional parameters.

TABLE OF CONTENTS

	Page
ABSTRACT.....	iv
LIST OF TABLES	ix
LIST OF FIGURES	x
NOMENCLATURE	xi
I INTRODUCTION.....	1
1.1 Adsorption.....	2
1.2 Adsorbent.....	3
1.3 Metal-Organic Frameworks	3
1.4 Flexible Frameworks/MIL-53(Al)	4
1.5 Research Objective	5
II LITERATURE REVIEW	7
2.1 Breathing Behavior in MOFs.....	7
2.2 Transition during Breathing Phenomena	8
2.3 Effect of Synthesis Solvent on Breathing	8
2.4 Effect of History	9
2.5 Binary Equilibria Experimental Data.....	9
2.6 Adsorptive Separation.....	10
2.7 Modeling Flexible Framework Behavior.....	10
2.7.1 Stress Model.....	11
2.7.2 Osmotic Ensemble	12
2.7.3 Modified Dual Site Langmuir Model	13

2.7.4 Revised Dual Site Langmuir Model	14
2.8 Modeling of Flexible Frameworks for Binary Adsorption.....	15
2.8.1 Osmotic Framework Adsorbed Solution Theory (OFAST).....	16
III THEORY	18
3.1 Pure and Binary Gas Adsorption	18
3.2 Excess Adsorption	19
3.3 Langmuir Isotherm.....	19
3.3.1 Extended Langmuir Model	20
3.4 Grand Potential	20
3.5 Proposed model.....	21
IV MATERIALS AND METHODS	23
4.1 Synthesis	23
4.2 Characterization	24
4.2.1 Thermogravimetric analysis (TGA).....	24
4.2.2 BET Surface Area Analysis	25
4.3 Experimental Apparatus Description.....	26
4.3.1 Feed Section.....	26
4.3.2 Adsorption/Desorption Section.....	27
4.3.3 Bypass/Sampling section	27
4.3.4 Exit section.....	27
4.4 Preliminary Measurements	30
4.4.1 Preliminary Volume Measurements.....	30
4.4.2 Gas Chromatograph Calibration	33

4.5 Pure Component Isotherm Measurement.....	35
4.6 Binary Isotherm Measurements	37
V RESULTS AND DISCUSSION	39
5.1 Pure Component Adsorption Equilibria and Data Analysis	40
5.2 Pure Component Adsorption Equilibria Modelling.....	47
5.3 Binary Adsorption Equilibria Results and Data Analysis.....	48
5.3.1 Binary Adsorption Equilibria at Constant Pressure	49
5.3.2 Binary Adsorption Equilibria at Constant CO ₂ Composition	53
5.4 Binary Adsorption Equilibria Predictions.....	58
VI CONCLUSIONS AND RECOMMENDATIONS	59
6.1 Conclusions	59
6.2 Recommendations.....	60
REFERENCES	61
APPENDICES	
A: Propagation of error analysis in primary measurements.....	67
B: Pure Component Adsorption Equilibria Data on MIL-53(Al) at 293 K.....	69
C: Binary Adsorption Equilibria Data on MIL-53(Al) at 293 K	73

LIST OF TABLES

Table	Page
1: Helium Expansion Measurement Volumes	31
2: Section volumes of the custom-made volumetric system.....	33
3: GC calibration curve parameters	34
4: Gas Chromatograph run conditions	35
5: Binary Adsorption Equilibria Experimental Conditions	38
6: Model Parameters for CO ₂ Pure Component Adsorption Equilibria on MIL-53(Al) ..	47
7: Model Parameters for N ₂ Pure Component Adsorption Equilibria on MIL-53(Al)	48
B. 1 Pure CO ₂ experimental isotherm data on MIL-53(Al)lp at 293 K.....	69
B. 2 Pure CO ₂ experimental isotherm data on MIL-53(Al)np at 293 K.....	70
B. 3 Pure N ₂ experimental isotherm data on MIL-53(Al)lp at 293 K.....	71
B. 4 Pure N ₂ experimental isotherm data on MIL-53(Al)lp at 293 K.....	72
C. 1 Binary Adsorption equilibria experimental data on MIL-53(Al)np at 0.8 bar	73
C. 2 Binary Adsorption equilibria experimental data on MIL-53(Al)np at 1.3 bar	73
C. 3 Binary Adsorption equilibria experimental data on MIL-53(Al)np at 9.5 bar	74
C. 4 Binary Adsorption equilibria experimental data on MIL-53(Al)np at 0.20 y _{co2}	74
C. 5 Binary Adsorption equilibria experimental data on MIL-53(Al)np at 0.05 y _{co2}	75
C. 6 Binary Adsorption equilibria experimental data on MIL-53(Al)lp at 0.05 y _{co2}	75

LIST OF FIGURES

Figure	Page
1: lp and np structures of MIL-53(Al).	5
2: Thermal stability of MIL-53(Al)	25
3: Schematic Diagram of the custom-made Volumetric Adsorption System	29
4: Determination of the absolute volume of the adsorption/desorption section volume .	32
5: Calibration curve for Gas Chromatography Analysis.....	34
6: CO ₂ adsorption isotherm and model.....	40
7: CO ₂ adsorption capacity of MIL-53(Al) np and lp at sub-atmospheric pressures.....	43
8: N ₂ adsorption isotherm and model.....	44
9: Pure component adsorption capacity of CO ₂ and N ₂ on MIL-53(Al)np	46
10: Pure component adsorption capacity of CO ₂ and N ₂ on MIL-53(Al)lp	46
11: CO ₂ /N ₂ selectivity on MIL-53(Al)np at 0.8bar	49
12: CO ₂ /N ₂ selectivity on MIL-53(Al)np at 1.3bar	51
13: Effect of bulk gas composition on CO ₂ and N ₂ adsorption capacity of MIL-53(Al)np	51
14: Effect of molar composition on the adsorbed phase mole fraction.	52
15: Effect of pressure on the adsorption capacity of CO ₂ and N ₂	54
16: Difference in the binary adsorption characteristics of the np and lp phase	55
17: Effect of pressure on Adsorbed phase mole fraction.....	56
18: Effect of pressure on the selectivity of the np and lp phase of MIL-53(Al).....	57

NOMENCLATURE

b_i	Affinity parameter of phase I, bar^{-1}
b_{np}	Affinity parameter of the narrow pore phase, bar^{-1}
b_{lp}	Affinity parameter of the large pore phase, bar^{-1}
F_k	Helmholtz energy of phase k, kJ
K	Bulk modulus, kPa
K_H	Henry's constant, $\text{mol kg}^{-1} \text{bar}^{-1}$
m	Mean of the transition spreading pressure, Nm^{-1}
m_s	mass of adsorbent, g
N	Adsorption capacity, mol kg^{-1}
N_i	Adsorption capacity of specie I, mol kg^{-1}
N_0	Unit cell adsorption capacity, mol kg^{-1}
$N_{1\max}$	Narrow pore adsorption capacity, mol kg^{-1}
$N_{2\max}$	Large pore adsorption capacity, mol kg^{-1}
n_e	Excess amount adsorbed, mol kg^{-1}
n_t	Total amount of gas in the adsorption bed/column, mol kg^{-1}
P	Pressure, bar
P_{ext}	External pressure, bar
P_{i0}	Standard state pressure of specie I, bar
P_s	Solvation pressure, bar
P_{trans}	Transition pressure, bar
R	Gas constant, $\text{J mol}^{-1} \text{K}^{-1}$
S	Entropy, $\text{J K}^{-1} \text{g}^{-1}$

s	Standard deviation
ss	Stainless steel
T	Temperature, K
U	Molar internal energy, J mol ⁻¹
V, V _c	Volume, cell volume, cm ³
V _{empty}	Volume of the empty adsorption bed, cm ³
V _f	Final Volume, cm ³
V _k	unit cell pore volume, cm ³ g ⁻¹
V _{mi}	Molar volume of pure gas I, cm ³ mol ⁻¹
V _{0i}	Volume of section I, cm ³
V _{solid}	Volume of the adsorbent sample, cm ³
x _i	Mole fraction of specie i in the adsorbed phase at equilibrium
y _i	Mole fraction of specie i in the bulk gas phase

GREEK LETTERS

Ψ	Fraction of adsorbent sample in the large pore phase
ρ _c	Gas density at charge conditions, mmol cm ⁻³
ρ _e	Gas density at equilibrium, mmol cm ⁻³
ρ _g	Bulk gas density at equilibrium, mmol cm ⁻³
ρ _{mix}	Density of the gas mixture, mmolcm ⁻³
μ	Chemical potential, J mol ⁻¹

CHAPTER I

INTRODUCTION

This chapter provides a brief description of adsorption, adsorbents, metal-organic frameworks, and flexible frameworks. The objectives of this study are also stated.

Metal-organic frameworks (MOFs) are a rapidly growing class of nanoporous materials showing a very wide range of crystal structures and host-guest properties due to the tunable porosity, which is made possible by coordination chemistry and the versatility enabled by functionalization of organic linkers. It is expected that MOFs will have a major impact in many areas of science and technology¹. Some MOFs exhibit an exceptional flexibility and stimulus-responsive behavior,²⁻⁶ reacting to changes in temperature, pressure, and adsorption of guest molecules by undergoing structural transformations. Such materials have promising applications as sensors and actuators, as well as in adsorptive separation.^{3,5,7}

There are two distinct categories of stimulus-responsive MOFs. In one case, structural variations are progressive, as displayed in the case of the swelling of MIL-88 upon exposure to water and various alcohols.⁸ However, in other materials, the structural change is displayed by a relatively abrupt transition between two distinct structures of the framework. A particular example of MOFs exhibiting this bi-stability is the MIL-53

materials family,⁹⁻¹¹ which have recently attracted significant attention due to their prominent flexibility and the occurrence of a double, guest-induced structural transition (“breathing”) upon adsorption of certain gases.

1.1 Adsorption

Adsorption refers to the process in which porous solids bind large numbers of fluid molecules to their surface. This process plays a vital role in both separation and catalytic processes. Adsorption is a surface phenomenon that largely depends on the nature of the fluid and the adsorbing solid surface (typically, most useful adsorbents have very large surface area per unit mass).¹²

Furthermore, adsorption can be classified into two main categories: physical adsorption which is also referred to as “Physisorption” and chemical adsorption which is termed “Chemisorption”. Chemisorption involves the formation of chemical bonds between the adsorbent surface and the adsorbate molecule, hence chemisorption is an irreversible process. However, in the case of Physisorption, the adsorbate molecules are attached to the surface of the adsorbent due to Van der Waals forces. Therefore, physisorption is a reversible process. Adsorption is a temperature dependent process (The amount of a fluid specie adsorbed decreases with an increase in temperature). It is also noteworthy to state that adsorption is an exothermic process, consequently it is accompanied by the release of heat. The enthalpy of adsorption for physisorption is usually in the range of 10 to 40kJ/mol, while chemisorption has enthalpy changes in the range of 80 to 400 kJ/mol.¹³

1.2 Adsorbent

Adsorbent materials include traditional microporous materials like silica gel, activated alumina and activated carbon as well as crystalline aluminosilicates (zeolites) and metal-organic frameworks. Usually, adsorbents usually have peculiar properties that can be explored for applications. As an example, activated alumina, zeolites, silica gel and metal organic frameworks are hydrophilic and polar in nature, therefore they have a high affinity for polar molecules. On the contrary, activated carbon is non-polar in nature, as a result it shows no affinity towards polar molecules.¹⁴

The porosity of an adsorbent material is a very important property, typically the higher the porosity, the greater the surface area and pore volume of the adsorbent material. Usually, adsorbents can be categorized into three categories based on their pore sizes: microporous adsorbents (<2nm), mesoporous adsorbents (2-50nm) and microporous adsorbents (>50nm). The optimization of an adsorbents pore size is essential to ensure maximum utilization of its ability.

1.3 Metal-Organic Frameworks

Metal-organic Frameworks (MOFs) are a class of crystalline materials with ultrahigh porosity (up to 90% of free volume) and very high internal surface area of up to 6000m²/g. MOFs are made up of metal ions interconnected by organic linkers such as carboxylates, tetrazolates, sulfonates, etc. The extraordinary degree of variability with both the organic and inorganic parts of their structure makes MOFs of interest for several applications.¹⁵ MOFs are claimed to have potential for applications in areas such as clean energy including carbon dioxide capture, hydrogen storage, methane storage, membranes,

thin film devices, adsorption of vapours, separation of chemicals, drug delivery, catalysis, magnetism, polymerization, biomedical imaging etc.¹⁵⁻²²

1.4 Flexible Frameworks/MIL-53(Al)

Gas adsorption in porous solids has been observed to induce elastic deformation and has been reported in literature, dating back to the first experimental evidence of charcoal swelling by Meehan and Bangham.²³ However, because of the infinitesimal size of the strain (which ranges in the order of 10^{-4} - 10^{-3}), this effect has often been neglected²⁴. For nanoporous solids, the effect of adsorption deformation is not limited to swelling. For instance, zeolites and carbons, porous silicon and low-k films have all been observed to undergo contraction at low pressures followed by swelling at higher pressures²⁵.

A special class of metal-organic framework material referred to as MIL-53(M=Al or Cr) has drawn significant attention due to its enormous flexibility and its transition between two pore conformations termed “breathing” during adsorption. The two conformations are referred to as the large-pore phase (lp) and the narrow-pore phase (np).^{11,27-29} The cell volume of both conformations differ by up to 40%. At room temperature, and in the absence of guest molecules, the lp phase is the most stable form. However, in the process of adsorption of molecules such as CO₂ and H₂O, the lp phase transitions to the np phase at low pressures and reverses back to the lp phase at higher pressures. It has also been reported that the transition can be induced by the singular effect of temperature on the empty material. A considerable amount of research work has been published on this material because of its fascinating breathing behavior.^{6,9-11,25,28-31}

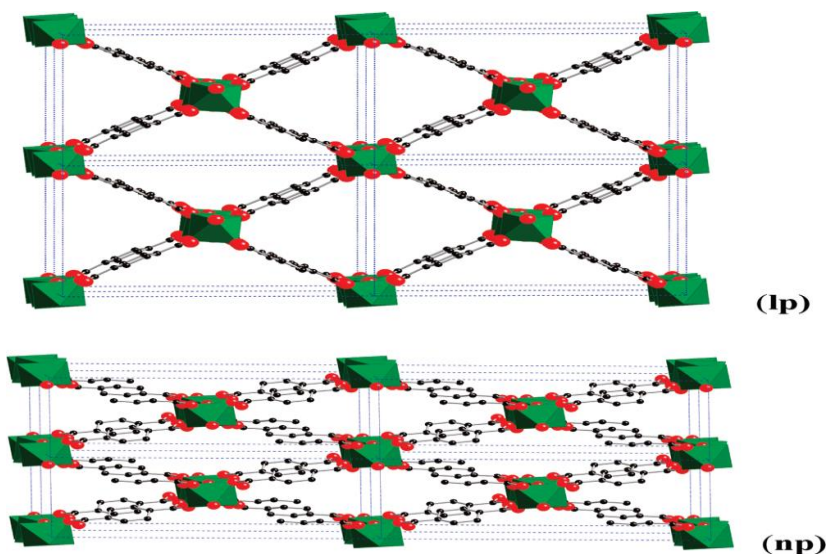


Figure 1: lp and np structures of MIL-53(Al).²⁵

1.5 Research Objective

Despite the fact that MIL-53(Al) has generated significant interest due to its breathing phenomenon, there exists a lack of binary equilibria data which would provide more insight into the adsorptive behavior of both the narrow and large pore phases. This will also elucidate the potential of this material for adsorptive separations. Consequently, this study aims to measure the pure and binary adsorption equilibria of CO₂ and N₂ on both phases of MIL-53(Al) to characterize their adsorption characteristics. In addition, a suitable yet simple model to predict the binary equilibria of CO₂/N₂ mixture based on their pure component adsorption properties will be developed. Such a model will include the dependence of adsorption isotherm on the history. We extend recently proposed history dependent pure component model (Edubilli,2018) to binary gas adsorption isotherms.

Thus, the novelty of this current study includes: provision of binary data set of CO₂/N₂ adsorption isotherm on the large as well as the narrow pore phase of MIL-53(Al) and the extension of the history dependent model to binary gas adsorption equilibria.

CHAPTER II

LITERATURE REVIEW

This section gives a brief overview of research studies on MIL-53(Al) that have investigated the rationale behind breathing phenomenon, number of transitions, effect of synthesis solvent, effect of history, and various approaches to modeling adsorption in flexible adsorbents.

2.1 Breathing Behavior in MOFs

In 2004, Loiseau et al.¹¹ studied the rationale behind the large breathing behavior of MIL-53(Al) upon hydration, this study utilized solid state NMR to analyze the hydration process. It was observed that the large breathing behavior of MIL-53(Al) upon hydration, was as a result of the hydrogen bonding interaction between the trapped water molecules and the oxygen atoms of the framework.

Also, In 2005 , Bourelly et al.²⁸ studied the adsorption of CO₂ and CH₄ on MIL-53(M=Al and Cr), and its isostructural vanadium (4⁺) MIL-47, at 304K with direct microcalorimetry measurements. It was observed that upon adsorption of CO₂ on MIL-53(M=Al and Cr) the material displayed the breathing phenomenon. However, the breathing phenomena were not observed for the adsorption of CO₂ on MIL-47 and CH₄ on MIL-53(Al and Cr). It was hypothesized that the breathing phenomenon is a result of

interactions between the CO₂ molecules and the hydroxyl component of the MIL-53 frameworks.

Lui et al. in 2008⁶ studied the reversible structural transition in MIL-53(Al). The study was conducted using neutron scattering and inelastic neutron scattering techniques. These authors established that MIL-53(Al) can undergo a large reversible structure transition as a function of temperature in the absence of any guest molecule. It was reported that the transition to the narrow pore conformation occurs around 125K-150K and the reverse transition to the large pore conformation occurs at around 325-375K. Furthermore, the study determined that the transition from the large pore to the narrow pore conformation had very slow kinetics.

2.2 Transition during Breathing Phenomena

In 2008 Coudert et al.³⁴ developed a thermodynamic model to describe guest induced structural transition in hybrid organic-inorganic frameworks. The model utilizes information from the adsorption isotherms to estimate the frameworks stability, number of transitions, and the pressure in which these transitions occur. The model proposed that MIL-53(Al) would undergo two structural transitions upon adsorption of CO₂, and it was concluded that the thermodynamics of the framework depends on the pore volume and adsorption affinity (Henry's constant).

2.3 Effect of Synthesis Solvent on Breathing

Walton et al.³¹ in 2015, studied the effect of synthesis solvent on the breathing behavior of MIL-53(Al). The study demonstrated that MIL-53(Al) synthesized in Dimethyl formaldehyde (DMF) at 120 °C does not undergo breathing upon adsorption of CO₂. This was attributed to the presence of uncoordinated BDC ligand which ensures the

material stays in the lp phase at all conditions. However, MIL-53(Al) synthesized in DMF at 220 °C demonstrated a very gradual breathing behavior which was not as abrupt as the breathing observed in the material synthesized under hydrothermal conditions. Both materials synthesized in DMF demonstrated an increased CO₂ uptake capacity in the pressure range of 1-5 bar indicating both materials remain in the lp phase upon adsorption of CO₂. Also, it was reported from NMR and FTIR studies that both MIL-53(Al) synthesized in DMF at 120 °C and 220 °C were unstable under humid conditions.

2.4 Effect of History

In 2013, Mishra et al.³⁵ demonstrated in their study that the adsorption characteristics of MIL-53(Al) is dependent on the adsorption history of the material. The study reported a procedure for tuning the lp phase to the np phase at ambient temperature by the adsorption of CO₂. MIL-53(Al) was also shown to remain in the np phase after desorption of CO₂. The study also demonstrated the increased CO₂ uptake capacity and the negligible N₂, CH₄, CO and O₂ uptake capacity of the np phase at sub-atmospheric. In this present study, we extend this effect of history on the adsorption characteristics of MIL-53(Al) to adsorption of a binary mixture of CO₂/N₂ at different conditions.

2.5 Binary Equilibria Experimental Data

In 2011, Ortiz et al.³⁰ conducted a study of the coadsorption of CO₂/CH₄ in MIL-53(Al). The coadsorption isotherms were measured at 253 K, 273K, 292 K and 323 K and at pressures ranging from 0-9.5bar. The total amount adsorbed was observed to increase with an increase in CO₂ molar composition for all conditions investigated. Also, the study reported that the evolution of the np-lp transition reopening pressure with CO₂ molar composition was non-monotonic. In addition, it was observed that a CO₂ molar

composition of less than 0.05 was able to trigger breathing in MIL-53(Al). The study demonstrated that the critical CO₂ composition required to induce breathing in MIL-53(Al), increased with temperature.

The above study provided the only available binary adsorption equilibria data on MIL-53(Al) in literature. Therefore, this present study aims to measure the binary adsorption equilibria of CO₂ /N₂ mixture (two very important gases in industrial applications, which are also the major constituent of flue gas) on MIL-53(Al).

2.6 Adsorptive Separation

In 2009, Finsy et al.³³ studied the separation of CO₂/CH₄ using a packed bed of MIL-53(Al) pellets. The separation of the binary mixture was investigated using breakthrough experiments at different binary mixture compositions with pressures ranging from 1-8bar. The study reported a higher CO₂ selectivity, compared to that of CH₄, over the entire pressure and concentration range. The selectivity was affected by the total pressure. In the pressure range of 1-5bar, the selectivity was relatively constant, and the separation factor had an average value of about 7. However, above 5bar the separation factor decreased to a value of 4.

2.7 Modeling Flexible Framework Behavior

A few researchers have proposed models to describe the behavior of flexible frameworks upon adsorption of guest molecules which induce structural transformation. In this section we review these models and elucidate on their limitations.

2.7.1 Stress Model

Neimark et al.²⁹ in 2010, proposed the stress model to describe the elastic deformation and structural transition that occur on MIL-53 as a consequence of adsorption induced stress (σ_s). σ_s is defined as the derivative of the grand thermodynamic potential (Ω_c) per unit volume with respect to the cell unit volume at constant temperature and chemical potential.

$$\sigma_s = \left(\frac{\partial \Omega_c}{\partial V_c} \right)_{T, \mu} \quad 2.7.1.1$$

The stress model proposes that the magnitude of the frameworks elastic deformation ε ($\varepsilon = \Delta V_c / V_c$, where ΔV_c is the variation of the cell volume) is determined by the Solvation pressure (P_s) which is defined as the difference between the adsorption stress and the external pressure as shown in the equation below

$$P_s = \sigma_s - p_{ext} = K_\varepsilon + \sigma_o \quad 2.7.1.2$$

where K is the bulk modulus and σ_o the pre-stress in the reference state.

The model hypothesizes that the structural transition occurs when the adsorption stress reaches a certain critical value σ^* , which the framework cannot resist. In the development of this model, the adsorption isotherms were assumed to follow a Langmuir isotherm. The adsorption stress σ_s can then be calculated by invoking the integral relationship between the grand thermodynamic potential and the adsorption isotherm.

$$\Omega_c = -RT \int_0^P N(p) \partial \ln p = -RT N_o \ln \left(1 + \frac{K_H P}{N_o} \right) \quad 2.7.1.3$$

where N_o is the unit cell capacity and K_H is the Henry constant.

$$\sigma S = RT \left\{ \left(\frac{dN_o}{dV_c} \right) \left[\ln \left(1 + \frac{K_H P}{N_o} \right) - \left(\frac{\frac{K_H P}{N_o}}{1 + \frac{K_H P}{N_o}} \right) \right] + \left(\frac{dK_H}{dV_c} \right) \left(\frac{P}{1 + \frac{K_H P}{N_o}} \right) \right\} \quad 2.7.1.4$$

In the case of MIL-53(AI) $\frac{dN_o}{dV_c}$ is positive while $\frac{dK_H}{dV_c}$ is negative leading to a non-monotonic variation in the adsorption stress (σS) and solvation pressure. The limitation of this model lies in the fact it assumes the structural transition occurs at a single pressure, however it has been shown from x-ray diffraction studies conducted by Llewellyn et al³⁶ that there exist regions where the np and lp phase co-exist implying the transition takes place over a pressure range. Furthermore, the change in amount adsorbed per unit cell per volume of unit cell $\left(\frac{dN_o}{dV_c} \right)$ and the change in Henry's constant per unit volume of unit cell $\left(\frac{dK_H}{dV_c} \right)$ cannot be determined experimentally.

2.7.2 Osmotic Ensemble

Coudert et al.³⁴ in 2008, proposed the use of the osmotic ensemble to rationalize the thermodynamics of adsorption on flexible frameworks when guest induced transition is involved. The osmotic potential is defined as:

$$\Omega_{os} = F_{khost}(T) + PV_k - \int_0^P N_{ads}(T, P) V_{mi}(T, P) \quad 2.7.2.1$$

Where F_{khost} (Helmholtz energy) is the free energy of the empty material, V_k is the unit cell pore volume of the given phase, N_{ads} is the amount of gas adsorbed as a function of temperature (T) and pressure (P) on the host phase and V_{mi} is the molar volume of the pure gas as a function of temperature and volume.

In order to determine the free energy difference between both phases, this approach fits the distinct part of the stepped experimental isotherm to obtain full rigid-host isotherms needed for both phases. The transition pressure is then estimated from the experimental isotherm and the difference in free energy of both phases is then estimated as follows:

$$\Delta F_{khost} = RT \int_0^{P_{trans}} \frac{\Delta N_{ads}(T,P) dp}{p} - P_{trans} \Delta V_{host} \quad 2.7.2.2$$

For conditions where adsorption isotherms are available at multiple temperatures, both internal energy and entropy differences, ΔU_{host} and ΔS_{host} , can be extracted from the free energies: $\Delta F_{host}(T) = \Delta U_{host} - T \Delta S_{host}$.

Also, the limitation of this approach lies in the fact that it assumes the transition occurs abruptly at a single pressure which is different from what have been observed experimentally from X-ray diffraction studies, which showed the co-existence of both phases. The fitting of the individual regions of the experimental stepped isotherm to model the adsorption characteristics of both rigid-host phases will introduce a high degree of uncertainty especially for the large pore phase which is modelled across the entire pressure range using only high-pressure data.

2.7.3 Modified Dual Site Langmuir Model

In 2014, Mishra et al.³⁷ modeled the structural transition (stepped adsorption isotherm) of MIL-53(Al) using a modified dual site Langmuir. The model incorporated an additional parameter (Ψ) to account for the degree of transition (pore opening) from the narrow pore to the large pore conformation as shown in the equation below.

$$N = \left(\frac{N_{1max} b_1 P}{1 + b_1 P} \right) (1 - \Psi) + \left(\frac{N_{2max} b_2 P}{1 + b_2 P} \right) (\Psi) \quad 2.7.3.1$$

Where N is the amount adsorbed, $N_{1\max}$ is the narrow pore saturation capacity, $N_{2\max}$ is the large pore saturation capacity, b_1 is the narrow pore affinity parameter, b_2 is the large pore affinity parameter, and P is the gas phase pressure.

Ψ was also defined to be a function of pressure and is defined mathematically as

$$\Psi = 1/2(1 + \operatorname{erf}\left(\frac{P-m}{\sqrt{2}s}\right)) \quad 2.7.3.2$$

Where m is the mean of the underlying Gaussian, and s is the standard deviation of the Gaussian. The advantage of this approach lies in the fact that it eliminates the need to estimate the Henry's constant and adsorption isotherm of the large pore conformation from high pressure data. Moreover, it accounts for the coexistence of the narrow and large pore conformations as reported in literature.

2.7.4 Revised Dual Site Langmuir Model

In 2018, Edubilli.³⁸ revised the Modified Dual Site Langmuir model and proposed that the pore opening parameter is a function of the spreading pressure difference between the large pore and narrow pore phases rather than pressure. Also, the history dependence of the adsorption isotherm was incorporated into the pore opening parameter. The revised dual site Langmuir model equations are described as follows:

$$N = \left(\frac{N_{1\max} b_{np} P}{1 + b_{np} P}\right)(1 - \Psi) + \left(\frac{N_{2\max} b_{lp} P}{1 + b_{lp} P}\right)(\Psi) \quad 2.7.4.1$$

$$\pi = \int_0^P \left(\frac{N}{p}\right) dp \quad 2.7.4.2$$

$$\pi_{lp} = N_{2\max}(1 + b_{lp} P) \quad 2.7.4.3$$

$$\pi_{np} = N_{1\max}(1 + b_{np} P) \quad 2.7.4.4$$

$$\delta = \pi_{lp} - \pi_{np} \quad 2.7.4.5$$

Where (Case 1) $\delta < 0$

$$\Psi_{est} = 1 - 0.5 \left(1 + \operatorname{erf} \left(\frac{\operatorname{abs}(\delta) - m}{\sqrt{2}s} \right) \right) \quad 2.7.4.6$$

$$\Psi = \min(\Psi_{est}, \Psi_o) \quad 2.7.4.7$$

Where (Case 2) $\delta > 0$

$$\Psi_{est} = 0.5 \left(1 + \operatorname{erf} \left(\frac{\operatorname{abs}(\delta) - m}{\sqrt{2}s} \right) \right) \quad 2.7.4.8$$

$$\Psi = \max(\Psi_{est}, \Psi_o) \quad 2.7.4.9$$

Where N is amount adsorbed(capacity), $N_{1\max}$ is the saturation capacity of the narrow pore phase, $N_{2\max}$ is the saturation capacity of the large pore phase, b_{np} is the affinity parameter of the narrow pore phase, b_{lp} is the affinity parameter of the large pore phase, P is the pressure of the bulk gas, Ψ is the fraction of the sample in the large pore phase. π is the spreading pressure, δ is the spreading pressure difference between the large and narrow pore phase, Ψ_{est} is the estimated fraction in the large pore phase and Ψ_o is the initial fraction in the large pore phase, m is the mean of the Gaussian and s is the standard deviation of the Gaussian.

2.8 Modeling of Flexible Frameworks for Binary Adsorption.

The widely accepted technique for predicting multicomponent adsorption on flexible adsorbents has been the Osmotic Framework Adsorbed Solution Theory (OFAST) proposed by Coudert et al. in 2010.³⁹ In this section, the application of OFAST to multicomponent adsorption on flexible adsorbent is described. Also, the limitations of OFAST are highlighted, and a different modeling approach based on a revised dual Langmuir is proposed.

2.8.1 Osmotic Framework Adsorbed Solution Theory (OFAST)

The Osmotic Framework Adsorbed Solution Theory is used to predict the evolution of structural transition and selectivity in fluid gas mixtures from experimental adsorption isotherms. The model has four control parameters which are the number of molecules on the host framework (N_{host}), the mechanical constraint (in this case the pressure (P)), Temperature (T), and the partial molar volume of specie i (V_{mi}).

The model defines an osmotic grand potential by the equation:

$$\Omega_{os} = F_{k\text{host}}(T) + PV_k - \int_0^P \sum_i N_{i(k)}(T, P, y) V_{mi}(T, P, y) dp \quad 2.8.1.1$$

For the special case of an ideal gas and an ideal mixture, the equation simplifies to

$$\Omega_{os} = F_{k\text{host}}(T) + PV_k - RT \int_0^P \frac{N_{T(k)}(T, P, y) dp}{p} \quad 2.8.1.2$$

Where $F_{k\text{host}}$ is the Helmholtz energy, V_k is the Volume of unit cell of the phase, $N_{i(k)}$ is the adsorbed quantity of fluid i (i.e. the partial co-adsorption isotherm) and $N_{T(k)}$ is the total quantity of fluid adsorbed.

Predicting multicomponent adsorption using OFAST involves fitting the experimental isotherm in the low-pressure region and high-pressure region to a model to represent the narrow pore and large pore region adsorption isotherms. Afterwards, the free energy difference between both phases is then determined by equating the grand potential of both phases at the transition pressure as shown in the equation 2.8.1.3

$$\Delta F_{k\text{host}} = RT \int_0^{P_{\text{trans}}} \frac{\Delta N_{i(k)}(T, P, y) dp}{p} - P_{\text{trans}} \Delta V_{\text{host}} \quad 2.8.1.3$$

The osmotic potential of the host phases is computed for all values of thermodynamic parameters of interest (pressure and gas mixture composition). This

enables the identification of the most stable phase (the phase with the lowest osmotic potential) at the pressure and composition of interest. The pressure at which the osmotic potential in both phases are equal is termed the “phase transition” pressure for a given composition. Finally, IAST is then used to compute the mixture adsorption properties of the most stable phase.

The limitation of this model lies in the fact that it assumes that the transition occurs at a single pressure, while X-ray diffraction studies have shown the co-existence of both phases.²⁹ Also, the technique of fitting the high pressure experimental isotherm data to a model to obtain the large pore phase adsorption isotherm introduces a high degree of uncertainty.

CHAPTER III

THEORY

This section gives an overview of some important adsorption theories. It discusses the concept of pure and binary adsorption equilibria, excess adsorption, grand potential, Ideal Adsorbed Solution Theory (IAST), Osmotic Framework Adsorbed Solution Theory (OFAST), and a revised dual site Langmuir model

3.1 Pure and Binary Gas Adsorption

The adsorption characteristics of an adsorbent material are described by adsorption isotherms. The amount of a pure gas (adsorbate) in equilibrium with an adsorbent at a constant temperature can be expressed as:

$$N = f\{P\} \quad (\text{constant } T) \quad 3.1.1$$

The above equation describes the amount of gas adsorbed by an adsorbent at equilibrium with the gas, as a function of the bulk gas Pressure (P) at a constant temperature. For a binary mixture the amount adsorbed is typically expressed as:

$$N_i = f\{P, y_i\} \quad (\text{constant } T) \quad 3.1.2$$

Where N_i = partial amount adsorbed of specie i. This indicates the partial amount of specie i adsorbed at equilibrium at a constant temperature, is a function of both the bulk gas pressure(P) and the mole fraction (y_i) of the bulk gas.

3.2 Excess Adsorption

In measuring excess adsorption volumetrically, a known mass (m_s) of an adsorbent is placed into a sample cell (adsorption column) of calibrated volume (V_{empty}). The adsorbent is then activated using high temperature or vacuum. A constant temperature is imposed by a temperature bath and a measured dose of gas (Δn) is introduced to the sample cell. When the system attains equilibrium, the temperature (T) and pressure (P) and composition (in the case of binary adsorption equilibria) are measured. The specific excess amount adsorbed (n_e) is defined by a mass balance:

$$n_e = \frac{n_t - \rho_g(V_{empty} - V_{solid})}{m_s} \quad 3.2.1$$

Where m_s is the adsorbent mass in the sample cell, V_d is the helium dead space of the sample cell (the volume helium would occupy in the sample cell at the given condition), ρ_g (T, P) is the density of the bulk gas obtained from an equation of state, and n_t is the total amount of gas in the sample cell. The helium dead space V_{solid} is obtained from a calibration with helium gas at ambient temperature (T_o) and pressure (P) before starting the experiment. This approach assumes that helium does not adsorb on the solid at ambient temperature.⁴⁰

3.3 Langmuir Isotherm

This is the simplest theoretical model for predicting monolayer adsorption. The Langmuir model is based on the assumptions that: molecules are adsorbed at a fixed

number of well-defined sites, each site can hold one adsorbate molecule, all sites are energetically equivalent, and there is no interaction between molecules adsorbed on neighboring sites. Mathematically the Langmuir model can be described as follows:

$$N = \frac{N_{max}bP}{1+bP} \quad 3.3.1$$

Where N is the amount adsorbed, N_{max} is the saturation capacity, b is the affinity parameter and P is the total Pressure.

3.3.1 Extended Langmuir Model

The Langmuir model can be extended to binary or multicomponent adsorption equilibria prediction. However, for this model to be thermodynamically consistent, the saturation capacity of the individual gases (N_{max}) must be equal. The extended Langmuir model can thus be described mathematically as:

$$N_i = \frac{N_{max}b_iP}{1+\sum b_iy_iP} \quad 3.3.1.1$$

Where N_i is the coadsorbed amount of specie i , N_{max} is the saturation capacity, b_i is the affinity parameter of specie i , y_i is the mole fraction of specie i in the bulk gas phase and P is the total Pressure.

3.4 Grand Potential

The grand potential plays a major role in adsorption thermodynamics. The grand potential is defined by:

$$\Omega = F + \int_0^P \sum_i u_i n_i = -PV \quad 3.4.1$$

Where Ω is the grand potential, F is the Helmholtz free energy of the fresh adsorbent (the adsorbent with no fluid molecule adsorbed on its surface), u_i is the chemical potential of specie i and n_i is the number of moles of specie i adsorbed. The

independent variables of the grand potential are temperature, volume, and chemical potential. These variables are precisely what is required to describe the amount adsorbed from a bulk gas at specified values of temperature and chemical potential in a solid adsorbent of fixed volume.

For the adsorption of a pure gas, the grand potential can be expressed as

$$\Omega = -RT \int_0^P \frac{n_i}{p} dp \quad 3.4.2$$

Physically, the grand potential can be described as the change in free energy associated with immersing an activated adsorbent in a bulk fluid.⁴¹

3.5 Proposed model

In this work, the pure adsorption equilibria of CO₂ and N₂ on MIL-53(Al) were modelled using a revised dual site Langmuir model proposed by Edubilli (2018). Also, this model was extended for the first time to predict binary adsorption equilibria in this study

The extension of the model equations is described as follows:

$$N_i = \left(\frac{N_{1\max} b_{np_i} y_i P}{1 + \sum b_{np_i} y_i P} \right) (1 - \Psi) + \left(\frac{N_{2\max} b_{lp_i} y_i P}{1 + \sum b_{lp_i} y_i P} \right) (\Psi) \quad 3.5.1$$

Therefore

$$\pi_{lp} = N_{2\max} (1 + \sum b_{lp_i} y_i P) \quad 3.5.2$$

$$\pi_{np} = N_{1\max} (1 + \sum b_{np_i} y_i P) \quad 3.5.3$$

Where (Case 1) $\delta < 0$

$$\Psi_{est} = 1 - 0.5 \left(1 + \operatorname{erf} \left(\frac{\operatorname{abs}(\delta) - m}{\sqrt{2}s} \right) \right) \quad 3.5.4$$

$$\Psi = \min(\Psi_{est}, \Psi_o) \quad 3.5.5$$

Where (Case 2) $\delta > 0$

$$\Psi_{est} = 0.5 \left(1 + \operatorname{erf} \left(\frac{\operatorname{abs}(\delta) - m}{\sqrt{2}s} \right) \right) \quad 3.5.6$$

$$\Psi = \max (\Psi_{est}, \Psi_o) \quad 3.5.7$$

Where N_i is the partial amount of component i adsorbed, $N_{1\max}$ is the saturation capacity of the narrow pore phase, $N_{2\max}$ is the saturation capacity of the large pore phase, b_{npi} is the affinity parameter of the narrow pore phase for component i , b_{lpi} is the affinity parameter of the large pore phase for component i , y_i is the mole fraction of component i in the bulk gas, P is the pressure of the bulk gas, Ψ is the fraction of the sample in the large pore phase. π is the spreading pressure, δ is the spreading pressure difference between the large and narrow pore phase, Ψ_{est} is the estimated fraction in the large pore phase and Ψ_o is the initial fraction in the large pore phase, m is the mean of the Gaussian and s is the standard deviation of the Gaussian.

CHAPTER IV

MATERIALS AND METHODS

This section describes the techniques used to synthesize and characterize MIL-53(Al). Also, a detailed description of the experimental apparatus and experimental procedures are reported in this section. Lastly, preliminary measurements results are reported

For this study the adsorption characteristics of the large and narrow pore conformations of aluminum terephthalate (MIL-53(Al)) was investigated by measuring its CO₂ and N₂ pure component adsorption isotherms and the binary adsorption isotherm of the mixture [of the above stated gases. The MIL-53(Al) was synthesized hydrothermally and characterized using thermogravimetric analysis (TGA) and Brunauer–Emmett–Teller (BET) surface area analysis. In addition, the adsorption equilibria were measured volumetrically.

4.1 Synthesis

In this study, MIL-53(Al) was synthesized under hydrothermal conditions as prescribed by Loiseau et al¹¹. The material was synthesized using aluminum nitrate nonahydrate (Al(NO₃)₃·9H₂O), 1,4 Benzene dicarboxylic acid (BDC), dimethylformamide(DMF), and deionized water. Aluminum nitrate nonahydrate (Al(NO₃)₃·9H₂O), 1,4benzene dicarboxylic acid and deionized water with a molar ratio

of 1Al(78.1g),0.5BDC(17.3g):80 H₂O(300g) were placed in a batch reactor. Afterwards, the reactor was placed in an oven at a temperature of 220 °C under autogenous pressure for 72 hours. The resulting product was then centrifuged and washed in DMF. Afterwards, the sample obtained was placed in the batch reactor with 200 ml of DMF and the reactor was then placed in an oven for 15 hours at a temperature of 150 °C to remove the unreacted BDC. The sample obtained was washed three times in methanol (to replace DMF in the pores) and calcined for 16 hours at 280 °C. The yield of MIL-53(Al) was about 11 g for each of the 5 batches processed.

4.2 Characterization

The MIL-53(Al) sample was characterized using BET and TGA

4.2.1 Thermogravimetric analysis (TGA)

Thermogravimetric analysis (TGA) of synthesized MIL-53(Al) was performed in a thermogravimetric analyzer (Mettler TOLEDO, model no. TGA/SDTA 851e). The temperature was ramped from 25 to 580°C with a heating rate of 5 K min⁻¹, and the measurements were carried out under a nitrogen atmosphere. TGA results are shown in

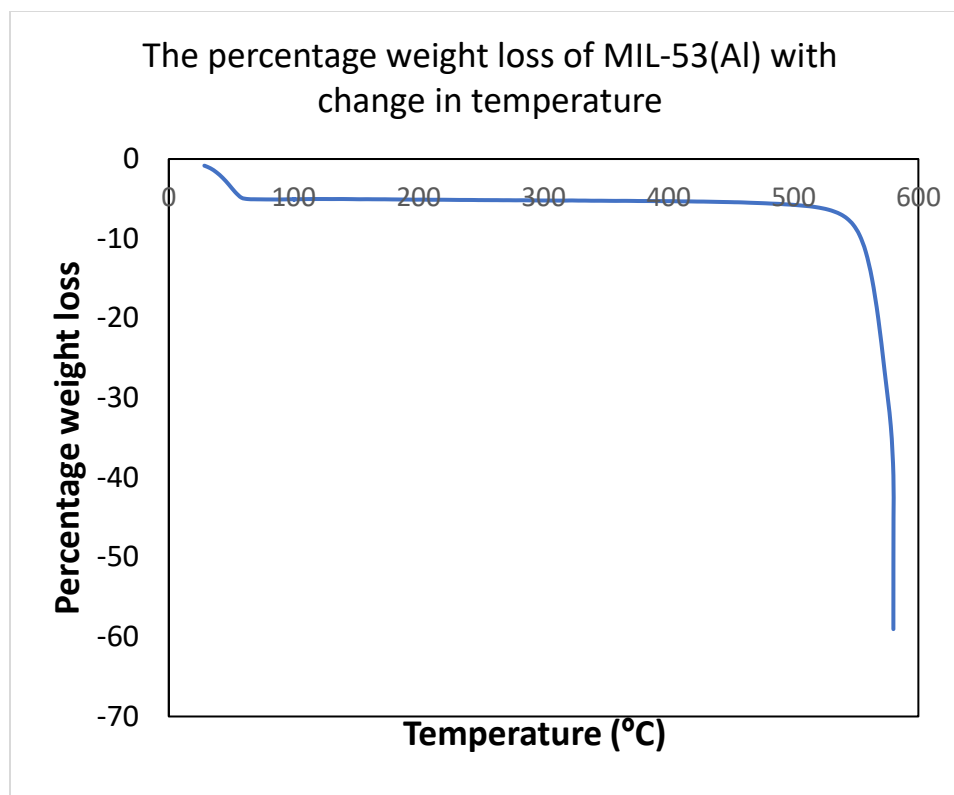


Figure 2: Thermal stability of MIL-53(Al)

Figure 2 which shows the MIL-53(Al) sample was stable up to 540 °C which is consistent with values reported in literature.

4.2.2 BET Surface Area Analysis

A micrometrics ASAP 2010 was used for nitrogen physisorption at 77 K. Prior to nitrogen physisorption, MIL-53(Al) sample was degassed at 493 K for 4 hours. The specific surface area was calculated using the Brunauer–Emmett–Teller (BET) model and relative pressure (P/P₀) range of 0.03–0.3 was used in its calculation. The pore volume was calculated at a pre-determined relative pressure (P/P₀) of 0.98. The BET surface area and pore volume were estimated to be 1284 m²/g and 0.64 cm³/g respectively, these estimates are in agreement with values previously reported in

literature.

4.3 Experimental Apparatus Description

A custom-made volumetric apparatus was used to conduct the gas adsorption measurements. A schematic diagram of this system is shown Figure 3 below. The system consists of a closed volume with a recirculation loop charged with the gases to be adsorbed. Also, the system is made up of different sections corresponding to the feed, adsorption/desorption, bypass/sampling and exit sections. In addition, the system is also connected to a gas chromatograph (GC) via a 6-way sampling valve to determine the gas phase composition at equilibrium in binary adsorption equilibria experiments.

4.3.1 Feed Section

The feed section consists of gas lines connected to a manifold. The gas manifold is connected to cylinders containing the gases of interest. The gases used in this study were nitrogen (Grade 5.0, >99.999%), carbon dioxide (Grade 4.4, >99.99%) and helium (Grade 4.7, >99.997%). The Feed Inlet section includes a small and a big tank, with internal volumes of 92.87cm³ and 157.65cm³ respectively, which were determined by helium expansion experiments (which are described in detail later). Additionally, the tanks are immersed in a water bath to maintain isothermal conditions. A J-Type thermocouple was immersed in the water bath for measuring the tanks' temperatures. As shown in Figure 4.2 valves A2, A4 and A3, A5 are inlet and outlet valves to the big and small tanks respectively, while the valve A13 connects the big and small tank. This valve is useful for mixing during binary adsorption equilibria measurements. The valves used in this study were B-type bellow valves, NUPRO SS-4BK.

4.3.2 Adsorption/Desorption Section

The adsorption/desorption section includes a changeable 20cm stainless steel adsorption column (1inch tubing) with 15.64grams (mass after activation) of MIL-53(Al) adsorbent. A J-type thermocouple was embedded in the column, which was placed in a water bath to serve as a temperature control mechanism. The water bath is connected to water circulator for maintaining isothermal conditions and stabilizing the column temperature within $\pm 0.1^{\circ}\text{C}$ accuracy throughout the experiments. valves A6 and A7 as shown in Figure 3 are the inlet and outlet valves to the column respectively, while valve A10 serves as a bypass of the column to the exit section.

4.3.3 Bypass/Sampling section

This section is mainly used for binary adsorption equilibria measurements and for circulating helium during activation of the adsorbent. The section consists of a pump, a mass flow controller, and a sampling valve for GC analysis. Usually, the pump is used for mixing gases and circulating the gas mixture throughout the system, including the column, to maintain a uniform composition when running binary gas experiments. The mass flow controller (model: 33 FMA123) has a range of 0-100sccm and is used to control the recirculation rate during binary experiments. It is also used to control the flow of Helium gas during activation of the adsorption column. The sampling valve is connected to an Agilent gas chromatograph system, which aids in the determination of the gas composition.

4.3.4 Exit section

This section is equipped with two pressure transducers for measuring the pressure in the system. One of the pressure transducers has a range of 0-15psi and is used to take

low pressure measurements due to its high degree of accuracy. However, the second transducer is used for taking high pressure measurements and has a range of 0-10340torr (200psi). These pressure transducers are enclosed by four pressure gauge valves (P1, P2, P3, P4) which are H-type compact rugged bellow valves, NUPRO SS-2H. Valve A11 serves as the main exit from the system and is connected to a vacuum pump (Fisher Scientific Maxima C Plus M2c 0125777 115/230v 60hz) with a rating of 0.002*torr*.

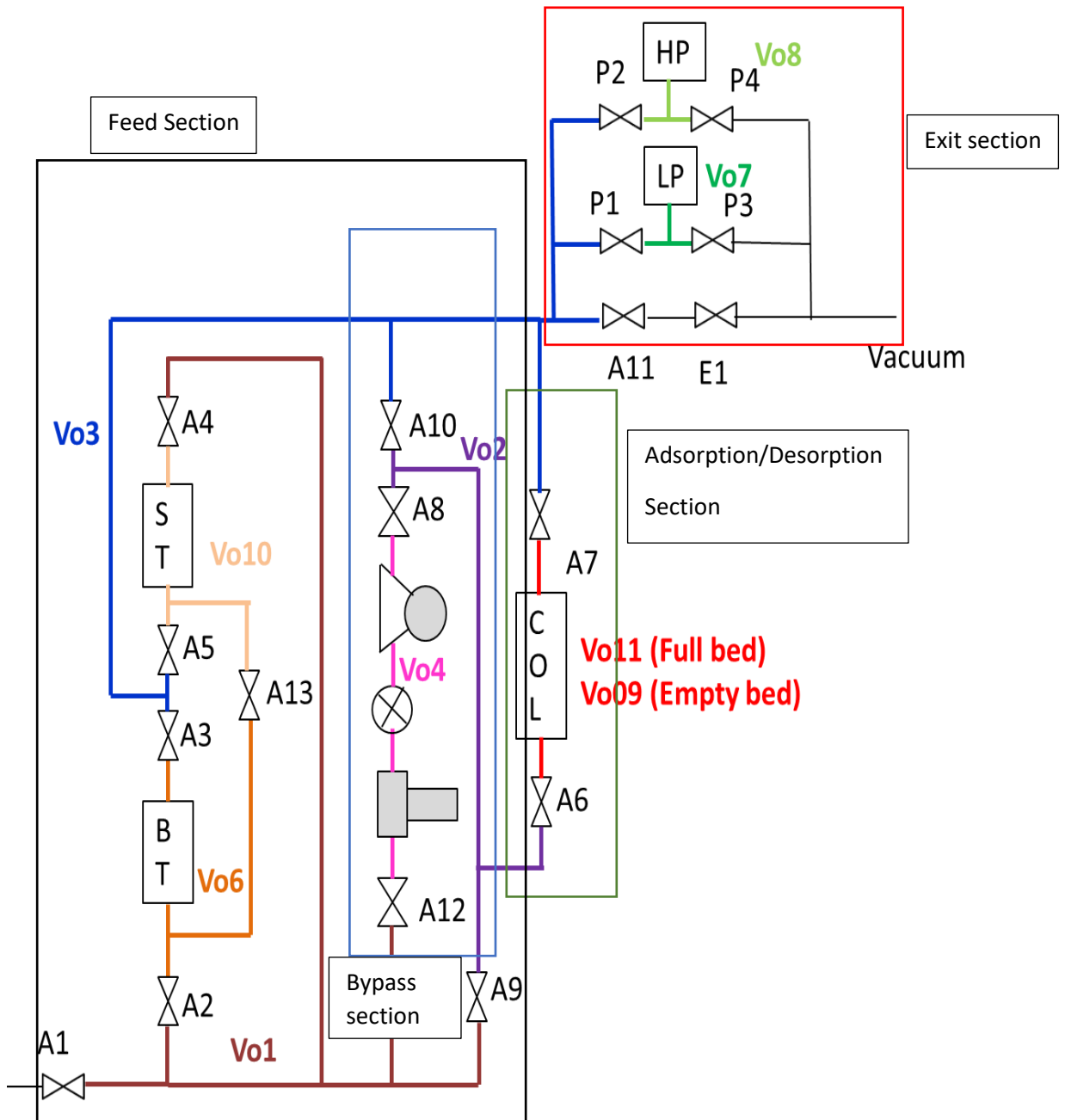


Figure 3: Schematic Diagram of the custom-made Volumetric Adsorption System

A1- Feed Inlet	A7-Bed/Column Top	A13- BT and ST Connector
A2- Big-tank Inlet	A8-Pump/Side Branch Out	P1- Low Pres. Trans. In
A3- Big-tank (BT) Outlet	A9- Pump/Side Branch Bypass	P2-High Pres. Trans. In
A4- Small-tank (ST) Inlet	A10- Bed/Column Bypass	P3-Low Pres. Trans. Out
A5-Small-tank Outlet	A11-Exit/Vacuum	P4-High Pres. Trans. Out
A6-Bed/Column Bottom	A12- Pump/Side Branch In	

4.4 Preliminary Measurements

Before the actual experiments were done to measure the pure and binary adsorption equilibria, preliminary measurements were taken to determine the volumes of individual sections of the custom-made volumetric system. In addition, the GC was calibrated by injecting CO₂/N₂ gas mixtures with known compositions.

4.4.1 Preliminary Volume Measurements.

The various volumes were determined using helium expansion measurements to determine the ratios between the volumes of each section of the system. This was done by charging a known amount of helium gas into a given section (V_{oi}) (the pressure and temperature in V_{oi} was recorded). The helium gas was then expanded into a chosen volume of the system (V_{oj}). The temperature and pressure after expansion was also recorded. The density of the helium gas before and after the expansion was determined using the Peng Robinson equation of state. Afterwards, the volume ratio was then determined by conducting a material balance as shown below

$$V_{oi}\rho_i + V_j\rho_j = (V_i + V_j)\rho_f \quad 4.4.1$$

$$m\rho_i + \rho_j = (m + 1)\rho_f \quad 4.4.2$$

$$\rho_f - \rho_j = m(\rho_i - \rho_j) \quad 4.4.3$$

Where ρ_i is the helium density in V_{oi} , ρ_j is the helium density in V_j before expansion, ρ_f is the helium density after expansion, and m is the ratio of V_i to V_j .

This procedure was repeated for all values V_{oi} and V_{oj} shown in Table 1.

Table 1: Helium Expansion Measurement Volumes

Volume(s) expanded from (V_{oi})	Volume(s) expanded to (V_{oj})
V_{o3}	V_{o8}
$V_{o2} + V_{o4}$	$V_{o3} + V_{o8} + V_{o10}$
V_{o2}	$V_{o3} + V_{o8} + V_{o10}$
V_{o1}	$V_{o2} + V_{o3} + V_{o8}$
V_{o2}	$V_{o3} + V_{o8}$
V_{o10}	$V_{o3} + V_{o8}$
V_{o9}	$V_{o3} + V_{o8}$
V_{o3}	V_{o8}
$V_{o2} + V_{o4}$	$V_{o3} + V_{o8} + V_{o10}$
V_{o3}	V_{o7}
V_{o4}	$V_{o2} + V_{o3} + V_{o8}$

Furthermore, the absolute volume of the system was determined using a combination of helium expansion experiments and stainless-steel balls (3mm diameter) of known mass and density. The density of the stainless-steel balls was determined in a Rubotherm microbalance to be 7.96 g/cm³. Afterwards, a known mass of the stainless-steel balls was placed in the column (adsorption/desorption section) and helium expansion measurements as were conducted from the column (V_{o9}) to volumes V_{o3} and V_{o8} . The procedure was repeated four times while varying the mass of the stainless-steel balls. The absolute volume of the column (V_{o9}) was determined as shown by the equation below

$$V_{ss} = -(V_{o3} + V_{o8})r + V_{o9} \quad 4.4.1.4$$

Where V_{ss} is the volume of stainless-steel balls in the column (V_{o9}) and r is the volume ratios determined from the helium expansion measurements. The plot of V_{ss} against r yielded V_{o9} as the intercept and the sum of volumes V_{o3} and V_{o8} as the slope as shown in Figure 4. The volumes of other sections of the system were then determined using this information in conjunction with the earlier determined volume ratios.

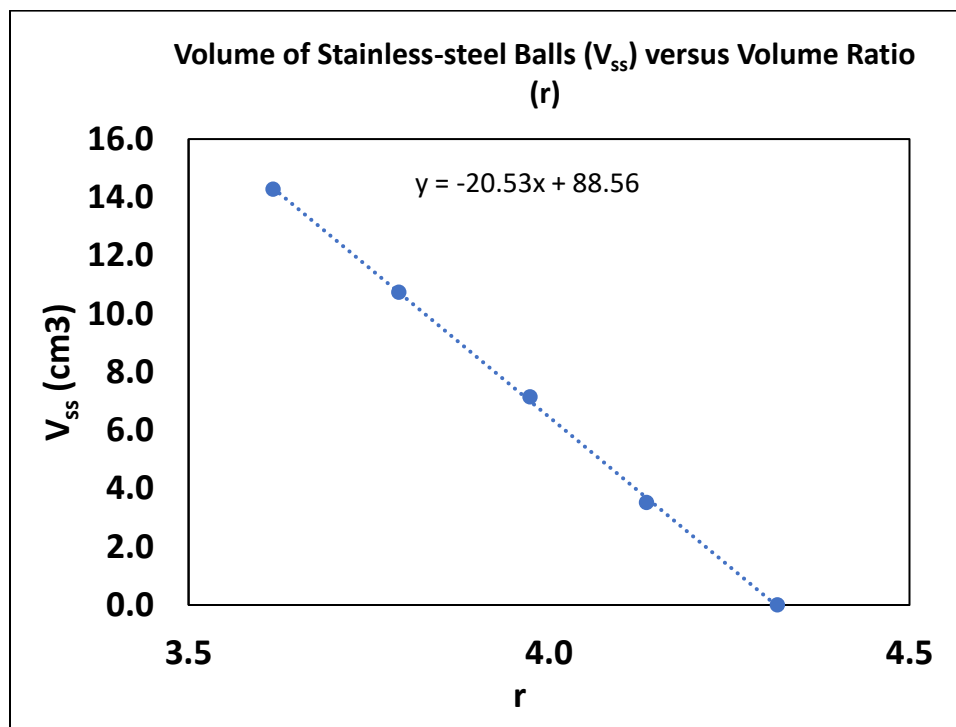


Figure 4: Determination of the absolute volume of the adsorption/desorption section volume

After the volume of each section of the system were determined, the column was filled with 15.64 g (mass after activation) of MIL-53(Al). Afterwards, helium expansion measurements were conducted to determine the volume of the filled bed. The volumes of the various sections of the volumetric system are reported in Table 2.

Table 2: Section volumes of the custom-made volumetric system

Volumes	(cm ³)	Standard error
Vo1	19.44	±0.03
Vo2	9.731	±0.010
Vo3	14.19	±0.01
Vo4	23.71	±0.03
Vo6	157.7	±0.1
Vo7	6.473	±0.021
Vo8	6.391	±0.016
Vo9 (bed empty)	88.56	±0.05
Vo10	92.87	±0.04
Vo11 (bed full)	78.26	±0.09

4.4.2 Gas Chromatograph Calibration

Gas Chromatography is used to separate/analyze components of a gas mixture to determine their relative compositions. In this study, a gas chromatograph with model number GC-system-Agilent 7890A was used in binary adsorption equilibria measurements to determine the gas phase compositions at equilibrium. Prior to starting the binary adsorption equilibria experiments, the gas chromatograph was calibrated by injecting mixtures of CO₂/N₂ with known compositions at a pressure of 2psia into the GC. A calibration curve was obtained relating the actual CO₂ mole fractions in the injected mixture to the corrected area per cent of CO₂ generated by the GC for the various gas mixture compositions. The calibration curve obtained is shown in Figure 5 below. In addition, the conditions of the GC runs are shown in Table 4.

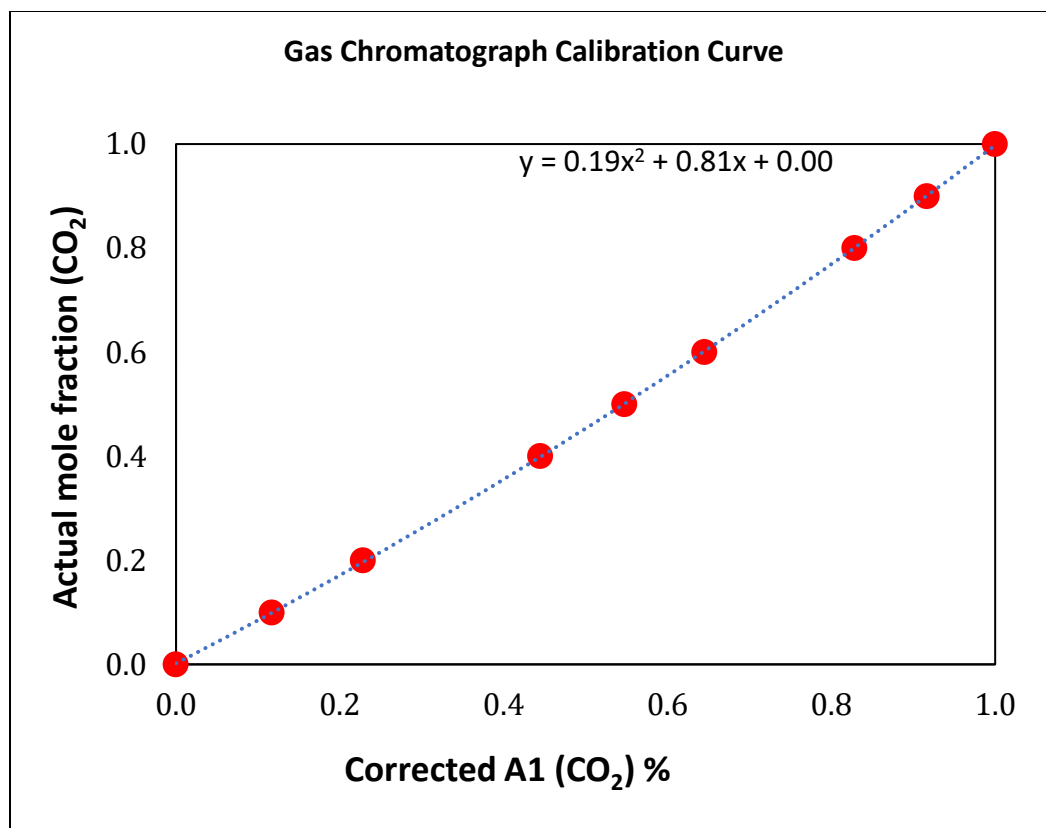


Figure 5: Calibration curve for Gas Chromatography Analysis

Table 3: GC calibration curve parameters

Parameter	Value	Standard Error
A	0.19	±0.007
B	0.81	±0.007
C	0.00	*Not significantly different from zero

Table 4: Gas Chromatograph run conditions

Detector	Thermal Conductivity Detector (TCD)
Carrier gas	Helium
Column	Hysep-D 10" by 180 SUPELCO 60/80
Detector temperature	200 °C
Oven temperature	50 °C
Helium flow rate	20 cm ³ min ⁻¹
Reference flow rate	40 cm ³ min ⁻¹
Make up flow rate	1 cm ³ min ⁻¹
Column pressure	21 psia

4.5 Pure Component Isotherm Measurement

The pure component isotherms of CO₂ and N₂ were measured on both the large and narrow pore conformations of MIL-53(AI). For the large pore conformation, the MIL-53(AI) sample placed in the column was activated by heating to a temperature of 220 °C and maintaining this temperature for about 3 hours. While activating the sample, helium is flown over the bed at a rate of 40 cm³/min to help improve the rate of heat transfer and purge. After activation, the column is immersed in a water bath and the temperature of the water bath is maintained at 20 °C (using a temperature-controlled water circulator connected to the water bath).

Upon completion of the above procedure, the large pore pure component isotherms were then measured by charging the gas of interest (CO₂ or N₂) into a section of the volumetric system (usually the small or big tank) to a given pressure. The gas is then expanded into the column and allowed to attain equilibrium (this occurs when the pressure remains constant for more than 30 minutes). The ambient and tank temperature of the charged gas are recorded. In addition, the ambient, tank and column temperature

and pressure of the gas at equilibrium were also recorded. The molar density of the gas charged and the density at equilibrium are then estimated using Peng Robinson equation of state. Afterwards, the total number of moles of the gas (n_t) in the column and the moles adsorbed per unit mass of MIL-53(Al) are determined from the material balance equations shown below

$$n_t = \rho_c V_c - \rho_e V_f \quad 4.4.2.1$$

$$n_e = \frac{n_t - \rho_g (V_{empty} - V_{solid})}{m_s} \quad 4.4.2.2$$

Where ρ_c (mmol/cm³) is the density of the gas at the charge condition, ρ_e (mmol/cm³) is the density of the gas at the equilibrium, V_c (cm³) is the volume of the charge section, V_f (cm³) is the volume the gas occupies at equilibrium excluding the column, n_e (mmol/g) is the excess amount adsorbed, ρ_g is the density of the bulk gas at the equilibrium condition (T,P) obtained from the Peng Robinson equation of state, and m_s is the mass of MIL-53(Al) in the column.

Afterwards, the column is then isolated, and the entire process is repeated for different equilibrium pressure ranges. In this study the isotherms were measured between 0-12 bar.

For the narrow pore isotherms measurements, the MIL-53(Al) sample in the column was charged with CO₂ to a pressure above 1bar and then the sample was desorbed by subjecting it to vacuum for about 3hours. This process leads to the transition from the large pore conformation to the narrow pore phase. After tuning the sample from the lp to the np phase, the isotherms measurements were conducted using the same procedure stated above for the large pore.

4.6 Binary Isotherm Measurements

The binary isotherm measurements were conducted on both the lp and np conformation. The procedure used for these experimental measurements were very similar to that of the pure component isotherm measurements. In the case of the lp conformation the MIL-53(AI) sample in the column was activated in the same way as was done for the pure component measurements. Afterwards, both the CO₂ and N₂ gas were charged to different sections of the volumetric system to predetermined pressures. Both gases were then mixed and circulated with the pump (bypass section) through the column until equilibrium was attained (each experiment took about 4 hours to attain equilibrium). The ambient, tank and column temperatures and pressure of the charge were recorded. In addition, the ambient, tank and column temperatures and the pressure of the gas were also recorded at equilibrium. Furthermore, at equilibrium, the pressure of the gas mixture was decreased to 2psia and a sample of the gas mixture was injected into the GC via the sampling valve to determine the gas phase compositions.

The total amount and partial amounts of the gas adsorbed in the column were determined using the material balance equations as shown below.

$$n_t = \rho_{CO_2} V_{CO_2} + \rho_{N_2} V_{N_2} - \rho_{mix} V_f \quad 4.4.2.3$$

$$n_{eCO_2} = \frac{x_{CO_2} n_t - \rho_{gmix} (V_{empty} - V_{solid})}{m_s} \quad 4.4.2.4$$

$$n_{eN_2} = \frac{x_{N_2} n_t - \rho_{gmix} (V_{empty} - V_{solid})}{m_s} \quad 4.4.2.5$$

Where ρ_{CO_2} is the density of CO₂ charged, V_{CO_2} is the volume charged with CO₂, ρ_{N_2} is the density of N₂ charged, V_{N_2} is the volume charged with N₂, ρ_{mix} is the density of

the gas mixture at the equilibrium, V_f is the volume occupied by the gas mixture at equilibrium excluding the volume of the column, x_{CO_2} is the CO₂ mole fraction at equilibrium, ρ_{gmix} is the density of the bulk gas mixture at the equilibrium condition (T,P) obtained from the Peng Robinson equation of state, and x_{N_2} is the N₂ mole fraction at equilibrium. The experimental conditions in which the binary adsorption equilibria measurements were conducted are listed in Table 5 below.

Table 5: Binary Adsorption Equilibria Experimental Conditions

Pressure (bar)	CO ₂ bulk gas Mole Fraction(y_{CO_2})	Phase
0.8	0.00 -1.00	np
1.30	0.00-1.00	np
9.50	0.00-1.00	np
0.00-6.00	0.20	np
0.00-9.00	0.05	np
0.00-8.00	0.05	lp

CHAPTER V

RESULTS AND DISCUSSION

This chapter reports the pure and binary adsorption equilibria experimental results.

Details of the modeling of the pure and binary isotherms using a revised dual-site

Langmuir model are also provided

Pure and binary adsorption equilibria data provide very useful insight on the potential of using a given adsorbent for adsorptive gas separations. In addition, for adsorbents that undergo a structural transformation upon adsorption of certain guest molecules, the pure and binary adsorption equilibria can provide additional information about the difference in the adsorption characteristics of the different phases of the different phases of the adsorbent material. In this chapter, the pure component adsorption equilibria of CO₂ and N₂ at 20°C on the lp and np MIL-53(Al) are reported. The binary adsorption equilibria of the CO₂/N₂ mixture on the np MIL-53(Al) at a constant temperature of 20°C, and constant pressures of 0.8bar, 1.3bar and 9.5bar are also reported. Additionally, binary adsorption equilibria data on MIL-53(Al) np at constant CO₂ gas phase composition of 0.05 and 0.2 and lp at constant CO₂ gas phase composition of 0.05 are reported as well.

5.1 Pure Component Adsorption Equilibria and Data Analysis

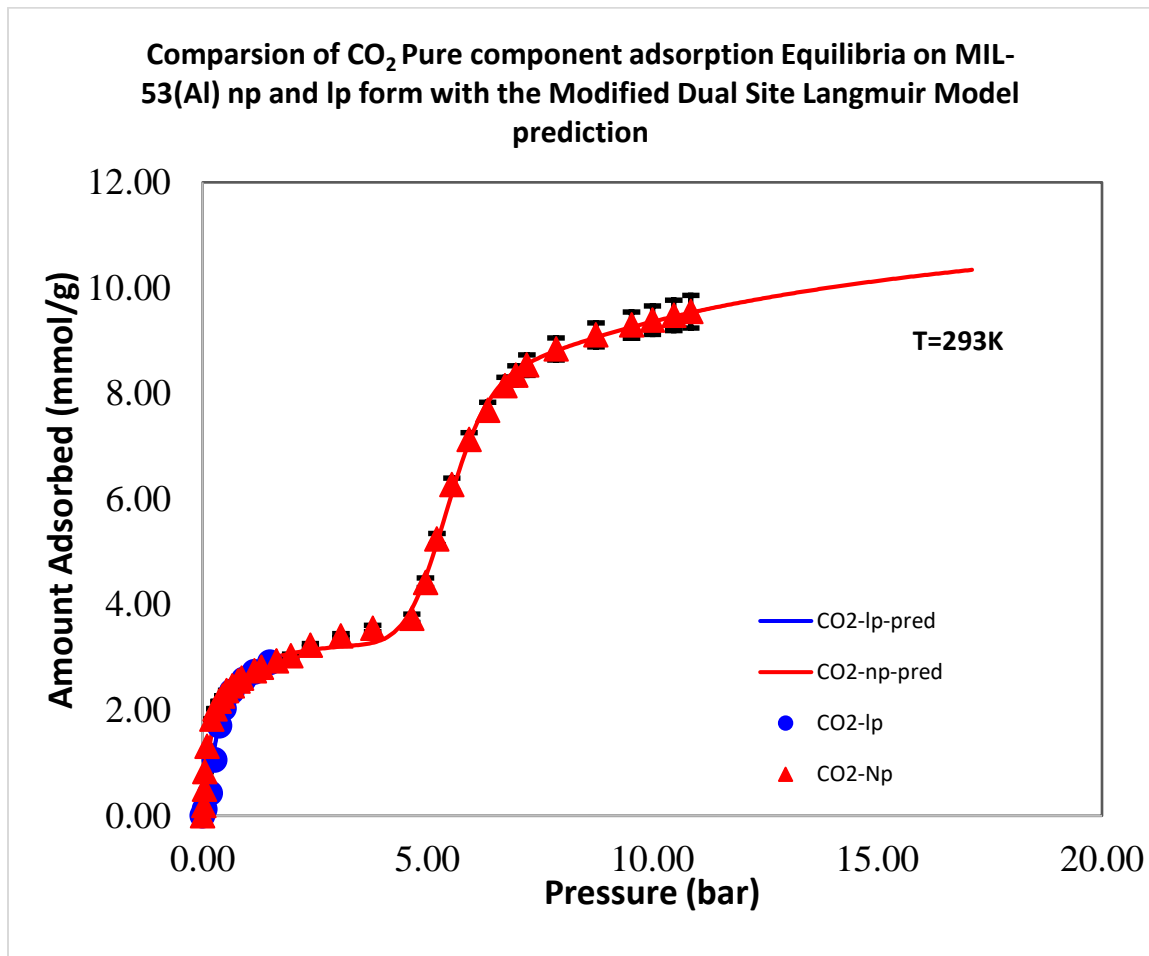


Figure 6: CO₂ adsorption isotherm and model

The pure component isotherm of CO₂ on MIL-53(Al) np at 20°C shows a step change in the isotherm at about 4.65 bar which occurs as a result of the np-lp structural transition induced by the interaction between CO₂ and the MIL-53(Al) sample. The sample is predominantly in the np phase for pressure ranges between 0-4.65 bar. Furthermore, at sub-atmospheric pressures (<1 bar), the CO₂ uptake capacity increased very steeply with a change in pressure which is indicative of the high CO₂ affinity of the np phase in this pressure range.

For pressures between 1-4.65 bar, the uptake capacity increased gradually from 2.74-3.74 mmol/g. However, at pressures greater than 4.65 bar (around the np-lp transition region), the CO₂ uptake capacity of the MIL-53(Al) sample increased significantly from 3.74 to 9.30 mmol/g when the pressure was varied from 4.65-9.54 bar. This demonstrates the high CO₂ adsorption capacity of the lp phase at higher pressures.

The characteristic adsorption behavior of MIL-53(Al) np described above, aligns with predictions of Coudert et al.³⁴ study ‘‘ Thermodynamics of guest induced transition in hybrid frameworks’’, which proposed that, for a framework with two metastable phases a single transition would occur when the pore volume of the starting phase is less than the pore volume of the second metastable phase. This implies that the phase with the lower pore volume would be the stable phase at lower pressures and the phase with the higher pore volume would be the stable phase at higher pressures.

In addition, this result is in good agreement with the pure CO₂ isotherms obtained by Boutin et al.²⁵ In their study, these authors found that the step change in the adsorption isotherm corresponding to the np-lp transitions occurs at about 2.5 bar for isotherms measured at 273 K and at 5 bar for isotherms measured at 298 K. In comparison, the step change in this present study occurred at 4.65 bar indicating that the np-lp transition of MIL-53(Al) is temperature dependent and the pressure range at which the transition occurs increases with temperature.

In the case of the adsorption equilibria of MIL-53(Al) lp, shown in Figure 6, the adsorption behavior is very similar to that of the np form at pressures greater than 1 bar. However, at sub-atmospheric pressures, the np phase displays a significantly higher CO₂ uptake capacity when compared with that of the lp phase. The difference in the

adsorption capacity of the np and lp form at sub-atmospheric pressures is shown more clearly in Figure 7.

It is hypothesized that this difference in the adsorption isotherms of the np and lp phase occurs because of the higher CO₂ affinity of the narrow pore form at sub-atmospheric pressures when compared with that of the large pore form. According to Coudert et al.³⁴, when the pore volume of the starting phase of the flexible framework (in this case the large pore conformation) is greater than that of the second metastable phase (narrow pore conformation), there is a probability that the framework will undergo two transitions (lp-np and np-lp) if the difference in the Helmholtz energy of both phases is small or when the affinity of the second metastable phase is high.

The lp phase undergoes a transition to the np phase in the pressure range of 0.17 - 0.92 bar as can be seen in Figure 7. Furthermore, at about 4.65 bar, the MIL-53(Al) begins another transition back to the lp phase as previously shown in Figure 6.

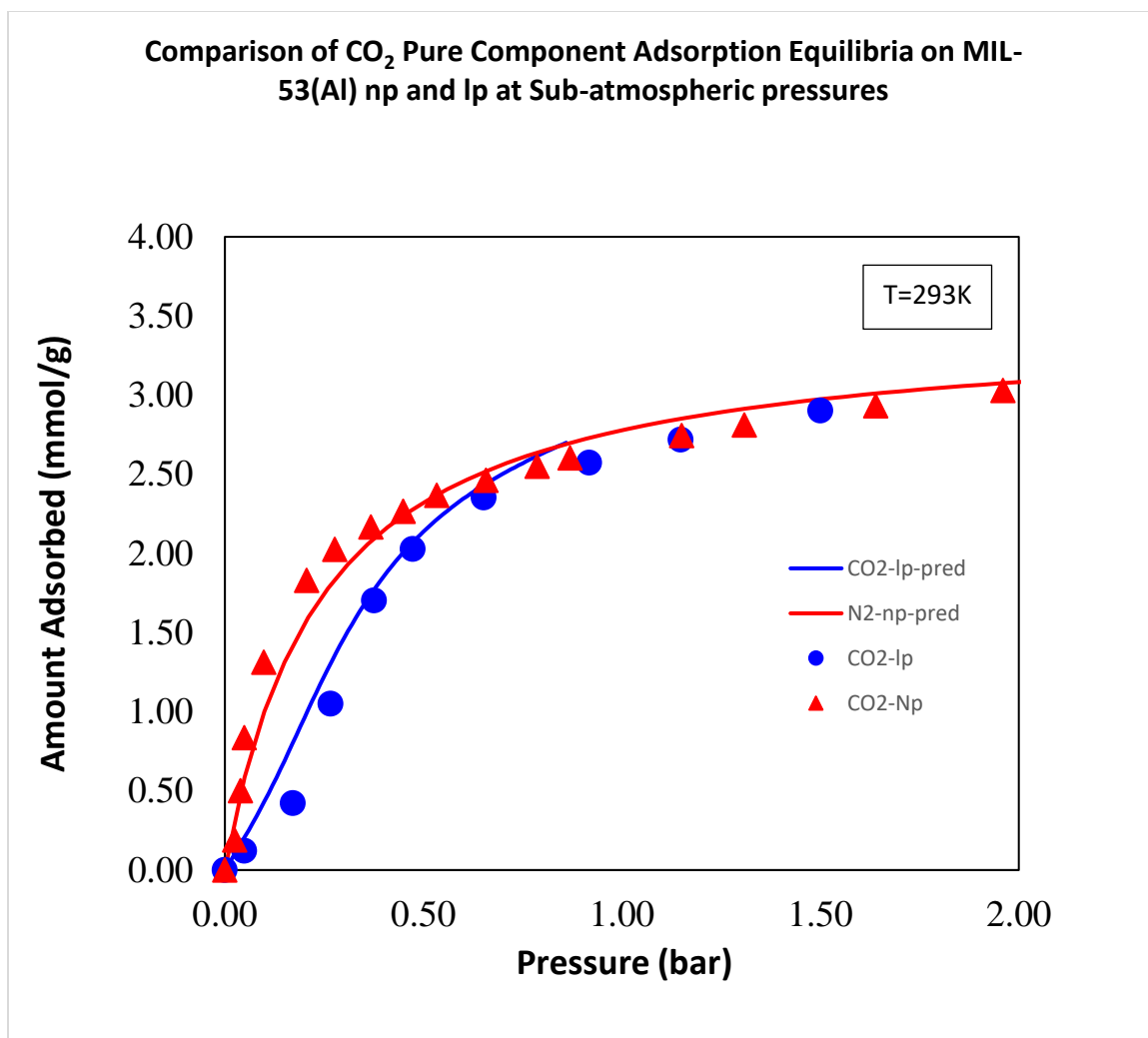


Figure 7: CO₂ adsorption capacity of MIL-53(Al) np and lp at sub-atmospheric pressures

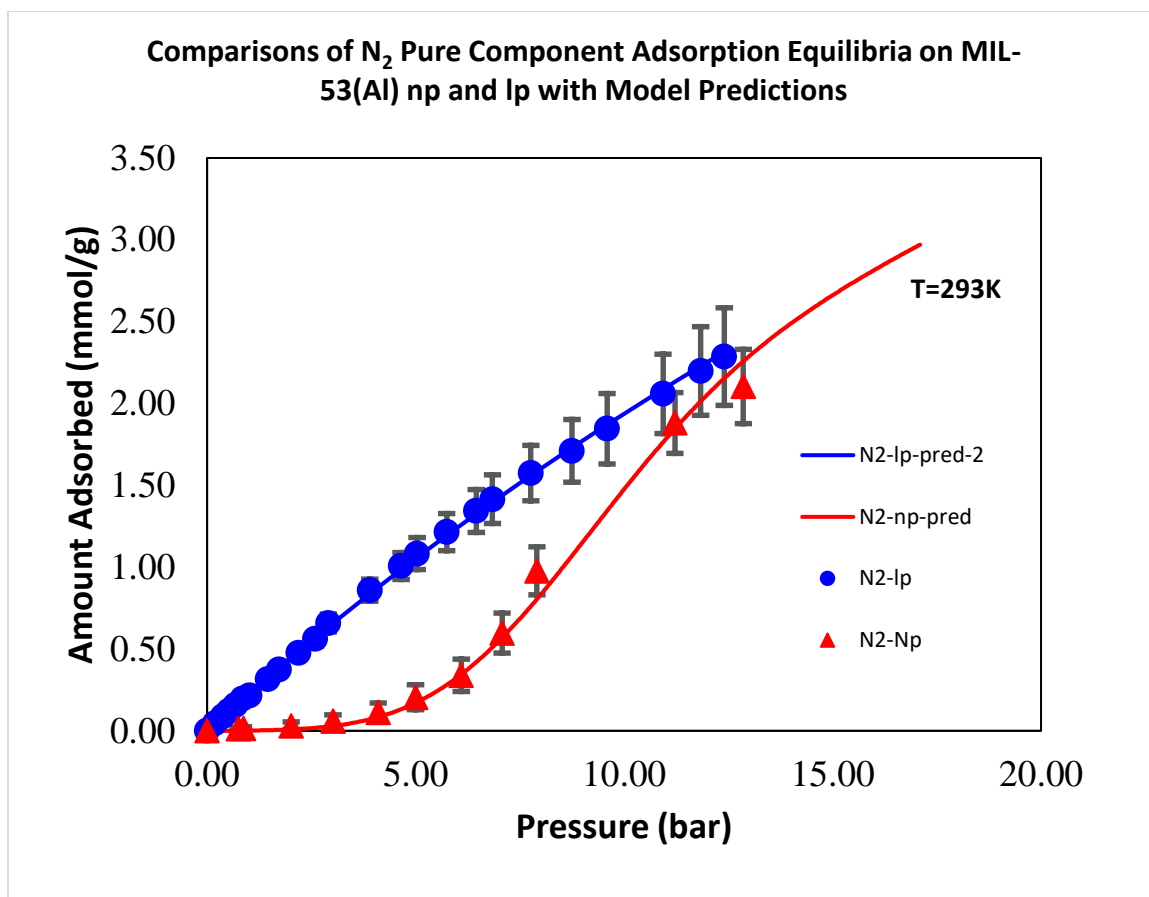


Figure 8: N_2 adsorption isotherm and model

The N_2 pure component adsorption equilibria on MIL-53(Al) np is shown in Figure 8. At pressures below 3 bar, the N_2 uptake capacity on the MIL-53(Al)np sample is negligible. However, at pressures greater than 3 bar, the N_2 uptake capacity begins to increase with increasing pressure. This happens probably because the sample is still in the np phase at pressures less than 3 bar and the np conformation probably has a negligible affinity for N_2 . However, at pressures greater than 3 bar, the MIL-53(Al) sample begins to undergo structural transition to the lp phase, which has a higher N_2 affinity, leading to an increase in the N_2 uptake capacity.

In addition, only one transition is observed, i.e. the transition from the np to the lp phase. This, again, is in agreement with predictions by Coudert et al.³⁴ as well as similar to results obtained by Mishra et al.³⁵ In the case of the N₂ pure component adsorption equilibria on MIL-53(Al) lp shown in Figure 8, the N₂ uptake capacity increases monotonically with increasing pressure. The MIL-53(Al) sample stays in lp phase for the entire pressure range (0-12bar). This implies the MIL-53(Al) lp sample did not undergo any structural transition upon adsorption of N₂. It is hypothesized that this happens because the lp conformation is the thermodynamically stable form both at low pressures, because of its higher affinity for N₂, and at high pressures, due to its greater pore volume in comparison with the narrow pore.

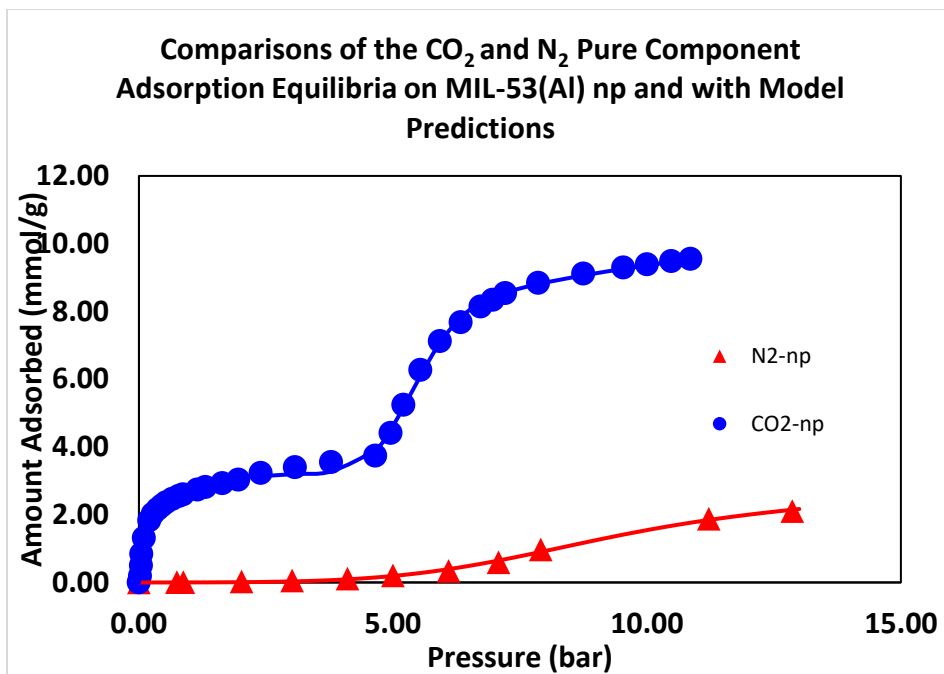


Figure 9: Pure component adsorption capacity of CO₂ and N₂ on MIL-53(Al)np

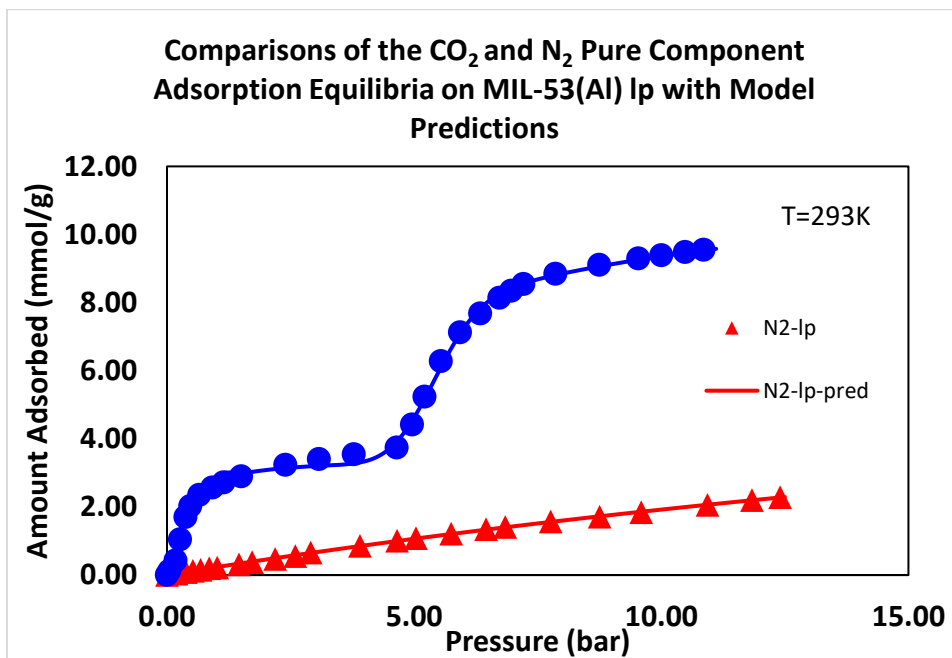


Figure 10: Pure component adsorption capacity of CO₂ and N₂ on MIL-53(Al)lp

5.2 Pure Component Adsorption Equilibria Modelling

The pure component adsorption equilibria of CO₂ and N₂ on MIL-53(Al)np and MIL-53(Al)lp were modelled using the revised dual site Langmuir model described earlier in chapter III. The model parameters were obtained by conducting a nonlinear regression using the least square method in the MATLAB curve fitting toolbox.

Table 6: Model Parameters for CO₂ Pure Component Adsorption Equilibria on MIL-53(Al)

Parameter	Value	Standard error
N _{1max} (mol kg ⁻¹)	3.5	± 0.06
b ₁ (bar ⁻¹)	4.1	±0.23
M	1.7	±0.07
S	0.6	±0.16
N _{2max} (mol kg ⁻¹)	12.1	±0.12
b ₂ (bar ⁻¹)	0.34	±0.011

The revised dual site Langmuir model provided a good fit of the pure component CO₂ adsorption isotherms of the MIL-53(Al)np and MIL-53(Al)lp. In the low-pressure region between 0.1-0.4 bar, the model under predicts the CO₂ adsorption capacity on MIL-53(Al)np and over predicts that of MIL-53(Al)lp. As discussed earlier, MIL-53(Al)lp undergoes two transitions upon adsorption of CO₂ in the pressure range studied in this work, and the revised dual site Langmuir model adequately modelled these transitions.

Also, the Henry's constant (which is a measure of an adsorbent's affinity for the gas of interest) of the narrow pore phase (14 molkg⁻¹bar⁻¹) is about 3.5 times greater than that of the large pore phase (4.1 molkg⁻¹bar⁻¹). Also, the saturation capacity of the large pore phase (12.1 molkg⁻¹) is about 3.5 times greater than the saturation capacity of the

narrow pore phase (3.5 mol kg^{-1}). This is probably due to the fact that the large pore phase has a larger pore volume than the narrow pore phase.

Table 7: Model Parameters for N₂ Pure Component Adsorption Equilibria on MIL-53(Al)

Parameter	Value	Standard Error
N _{1max} (mol kg ⁻¹)	3.5	± 0.06
b ₁ (bar ⁻¹)	0.0	* not significantly different from zero
m	1.7	±0.07
S	0.6	±0.16
N _{2max} (mol kg ⁻¹)	12.1	±0.12
b ₂ (bar ⁻¹)	0.02	±0.001

The revised dual site Langmuir model provided a good fit for the N₂ pure component adsorption equilibria on MIL-53(Al) and estimated the Henry's law constant for the narrow pore phase to be $0.0 \text{ mol kg}^{-1} \text{ bar}^{-1}$ and that of the large pore phase to be $0.02 \text{ mol kg}^{-1} \text{ bar}^{-1}$. In addition, the saturation capacity of the np was estimated to be 3.5 mol kg^{-1} for the narrow pore phase which is about 3.5 times less than that of the large pore phase estimated to be 12.1 mol kg^{-1} .

5.3 Binary Adsorption Equilibria Results and Data Analysis

As stated earlier, the binary adsorption equilibria in this study were measured at constant pressures of 0.8, 1.3 and 9.5bar. Also, measurements at constant CO₂ gas phase compositions of 0.05 and 0.20 were also done. All experiments were conducted at a constant temperature of 293 K. The results obtained, and their significance is presented below.

5.3.1 Binary Adsorption Equilibria at Constant Pressure

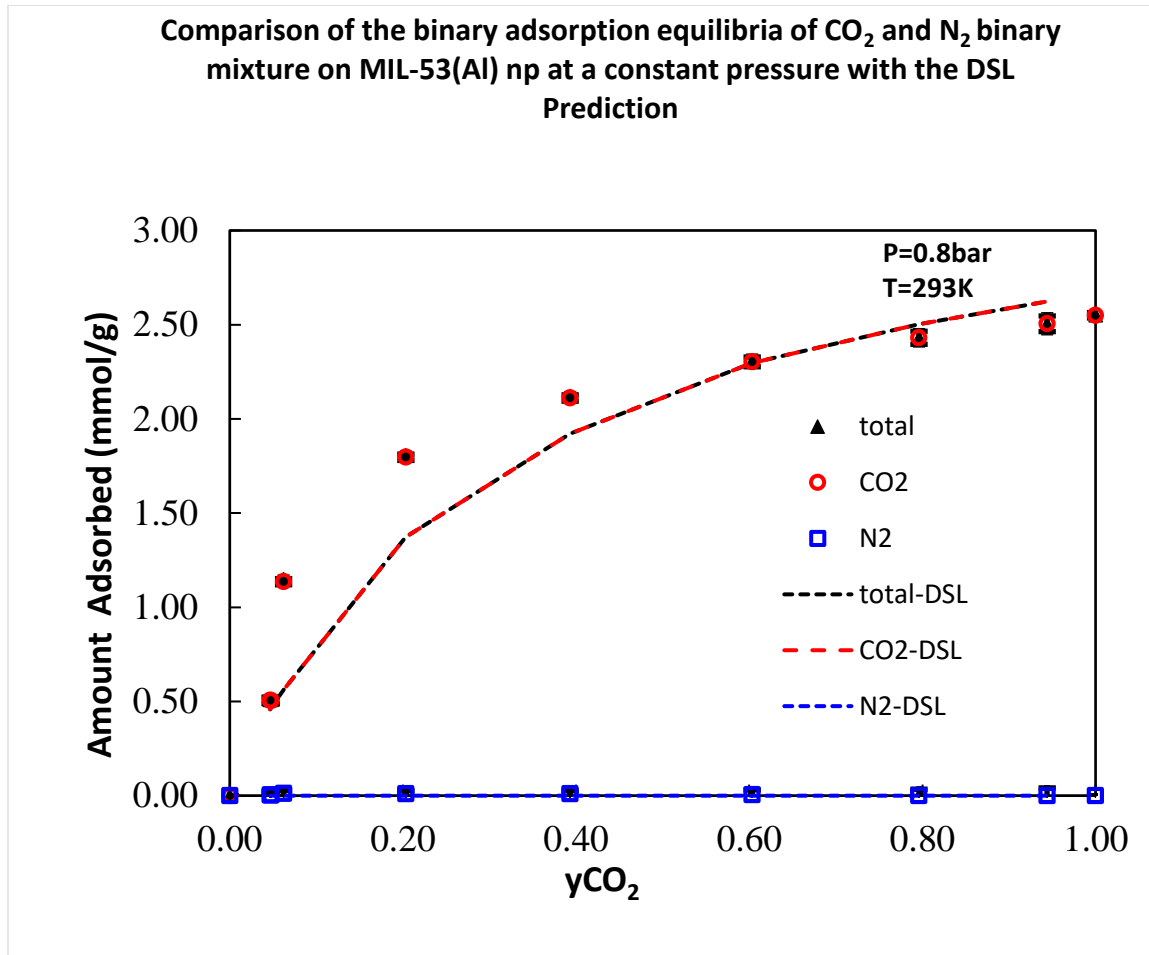


Figure 11: CO₂/N₂ selectivity on MIL-53(Al)np at 0.8bar

The constant pressure binary adsorption equilibria were measured at three different pressures of 0.8, 1.3 and 9.5bar . The plots of the adsorption capacity versus CO₂ mole fraction in the gas phase are presented in Figures 11, 12 and 13. The Isotherms measured at 0.8 bar and 1.3 bar show that the amount of N₂ adsorbed at these conditions is negligible. However, the CO₂ adsorption capacity increases with an increase in the CO₂ mole fraction. This results suggest that MIL-53(Al) np will be highly selective in separating a mixture of CO₂/N₂ at these conditions. Also, it is hypothesized that the MIL-53(Al) np stays in the narrow pore form under these conditions because the narrow pore

phase is the thermodynamically stable phase at low pressures. In addition, since the narrow pore phase has a high affinity for CO₂ and a negligible affinity for N₂ at pressures below 3 bar, the MIL-53(Al) np is thus highly selective in separating CO₂ from binary mixtures with N₂, at low pressures.

For the binary adsorption equilibria measured at 9.5 bar, the amount of N₂ adsorbed (capacity) decreases with an increase in the CO₂ mole fraction. At a CO₂ mole fraction of 0.053, approximately equal amounts of CO₂ and N₂ are adsorbed. However, as the CO₂ mole fraction is increased, the amount of CO₂ adsorbed increases, while that of N₂ decreases. At a pressure of 9.5 bar, the MIL-53(Al) sample is expected to be in the large pore phase, which is less selective towards separating CO₂ from the binary mixture when compared with the narrow phase. This is probably the underlying reason for the competitive adsorption between CO₂ and N₂ at low CO₂ mole fractions and, hence, the lower selectivity when compared with MIL-53(Al) in the narrow phase conditions described above.

In addition, Ortiz et al.³⁰ reported that no step change was observed in the partial amount of CO₂ adsorbed in the case of the binary adsorption isotherms of CO₂/CH₄ mixture on MIL-53(Al)lp measured at pressures greater than 8 bar and a temperature of 273 K, which suggest that under these conditions no transition occurs and MIL-53(Al) remains in the lp conformation. The binary adsorption equilibria of CO₂/N₂ mixture measured on MIL-53(Al)np at 9.5 bar and 293 K as shown in Figure 12 also did not show a step change in the partial amount of CO₂ adsorbed on the MIL-53(Al) sample. This observation further supports the fact that the lp conformation is the thermodynamically stable phase at high pressures.

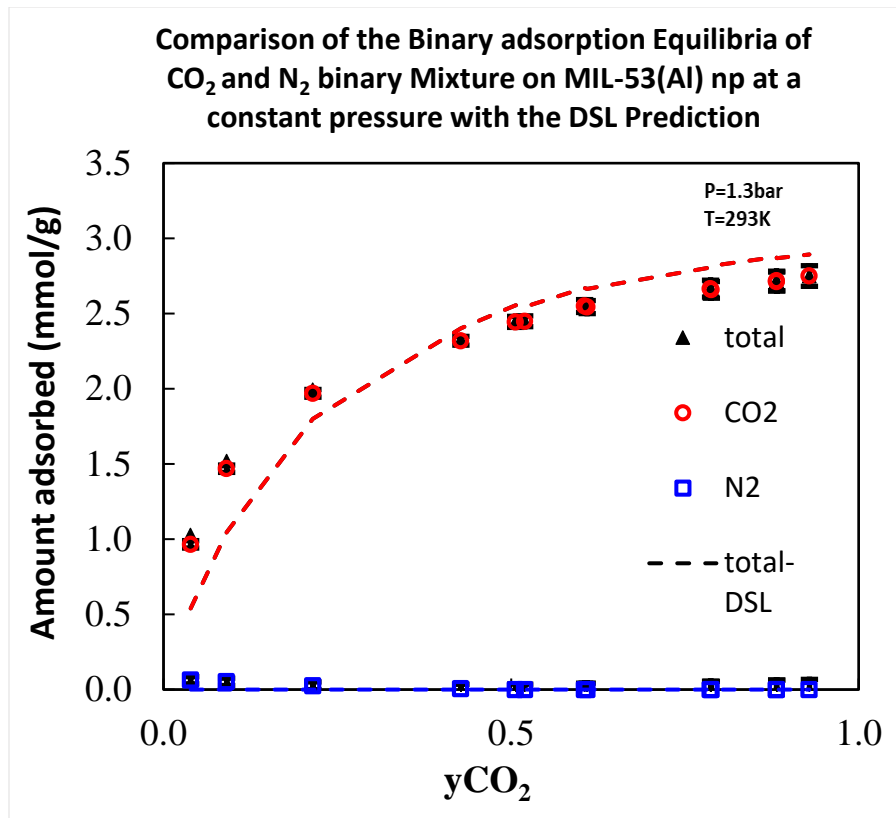


Figure 12: CO_2/N_2 selectivity on MIL-53(Al)np at 1.3bar

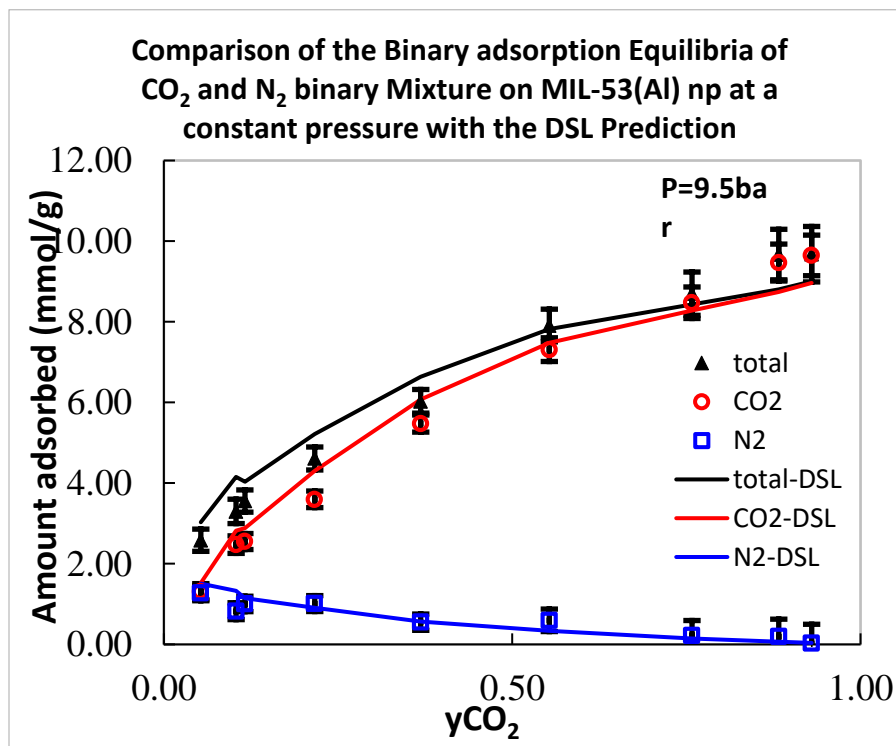


Figure 13: Effect of bulk gas composition on CO_2 and N_2 adsorption capacity of MIL-53(Al)np

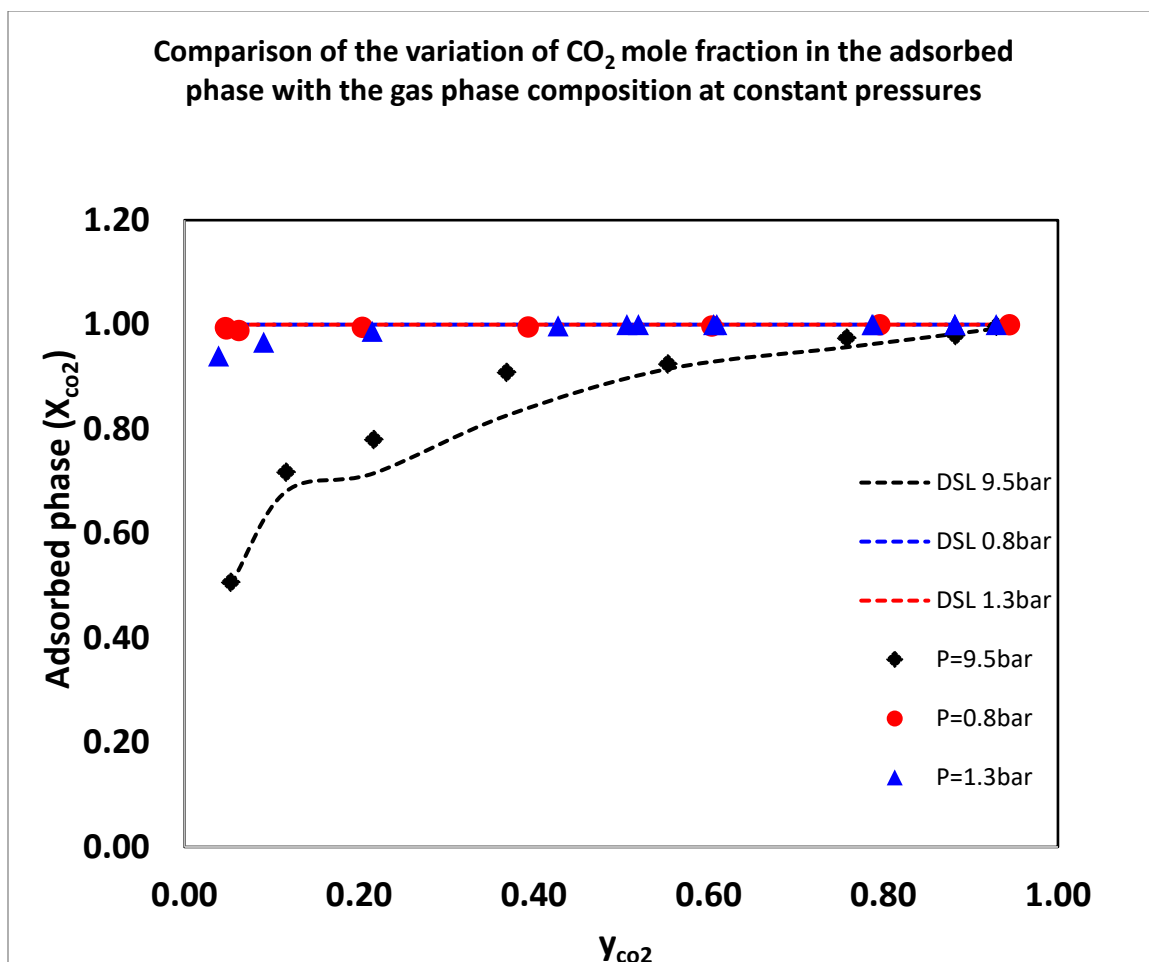


Figure 14: Effect of molar composition on the adsorbed phase mole fraction.

The variation of the CO₂ molar composition in the adsorbed phase with the CO₂ gas phase molar composition at constant pressures is shown in Figure 14. For the low pressures of 0.8bar and 1.3bar the CO₂ mole fraction in the adsorbed phase remained at a constant value of approximately 1 (indicating only CO₂ was adsorbed) regardless of the change in the CO₂ gas phase composition. For the high pressure (9.5 bar), the CO₂ mole fraction in the adsorbed phase increases with an increase in the CO₂ gas phase composition and approaches the low-pressure value at high CO₂ gas phase mole fraction of 1. This further supports the fact that the large pore phase is less selective in separating a CO₂/N₂ mixture with low CO₂ concentration.

5.3.2 Binary Adsorption Equilibria at Constant CO₂ Composition

Binary adsorption equilibria of the CO₂/N₂ mixture on MIL-53(Al) np and lp were measured to investigate the effect of pressure on the adsorption characteristic of both MIL-53(Al) phases. Three measurements were conducted. First, the binary adsorption equilibria were measured at a constant CO₂ composition of 0.20 on MIL-53(Al)np. The experiment was then repeated with the CO₂ composition held constant at 0.05. Afterwards, the binary adsorption equilibria were measured on MIL-53(Al) lp at a constant CO₂ composition of 0.05 to give further insight into the difference in the adsorption characteristic of both phases. The results are presented in Figures 15 and 16.

In the case of MIL-53(Al)np at constant CO₂ composition of 0.20 shown in Figure 15, the amount of N₂ adsorbed was negligible across the pressure range that was investigated. However, the CO₂ adsorption capacity increased with an increase in pressure. This is most likely because under this condition the MIL-53(Al) sample stays in the narrow pore phase which has a very high affinity for CO₂ and a negligible affinity for N₂.

For the experiments conducted on MIL-53(Al)np at constant CO₂ composition of 0.05 as shown in Figure 16, the amount of N₂ adsorbed was greater than that observed for the 0.20 constant CO₂ condition. However, the N₂ adsorption capacity was still negligible when compared with that of CO₂ at this condition. Lastly, the results of the binary adsorption equilibria measurements on MIL-53(Al)lp at constant CO₂ composition of 0.05 showed the adsorption of CO₂ and N₂ to be competitive at this condition, signifying that MIL-53(Al)lp is less selective for separating a mixture of CO₂ and N₂ at this condition.

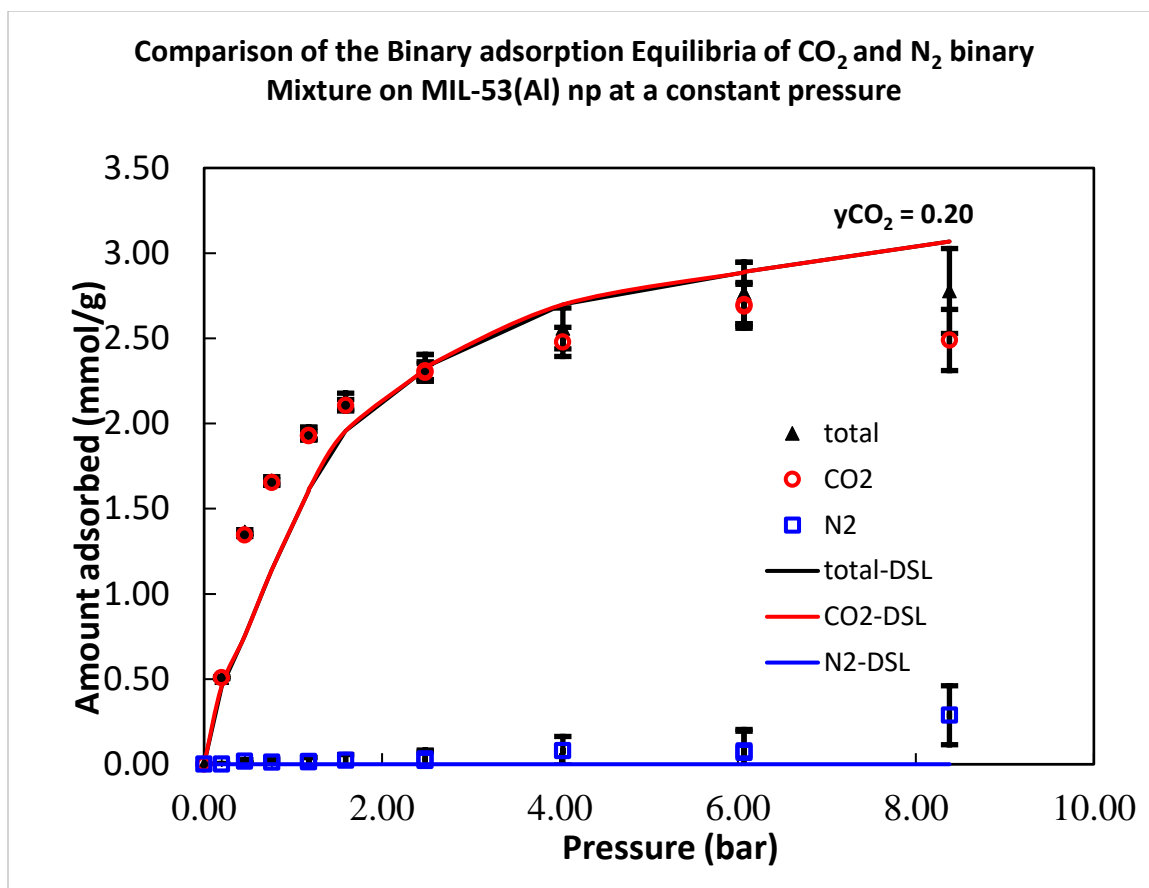


Figure 15: Effect of pressure on the adsorption capacity of CO₂ and N₂

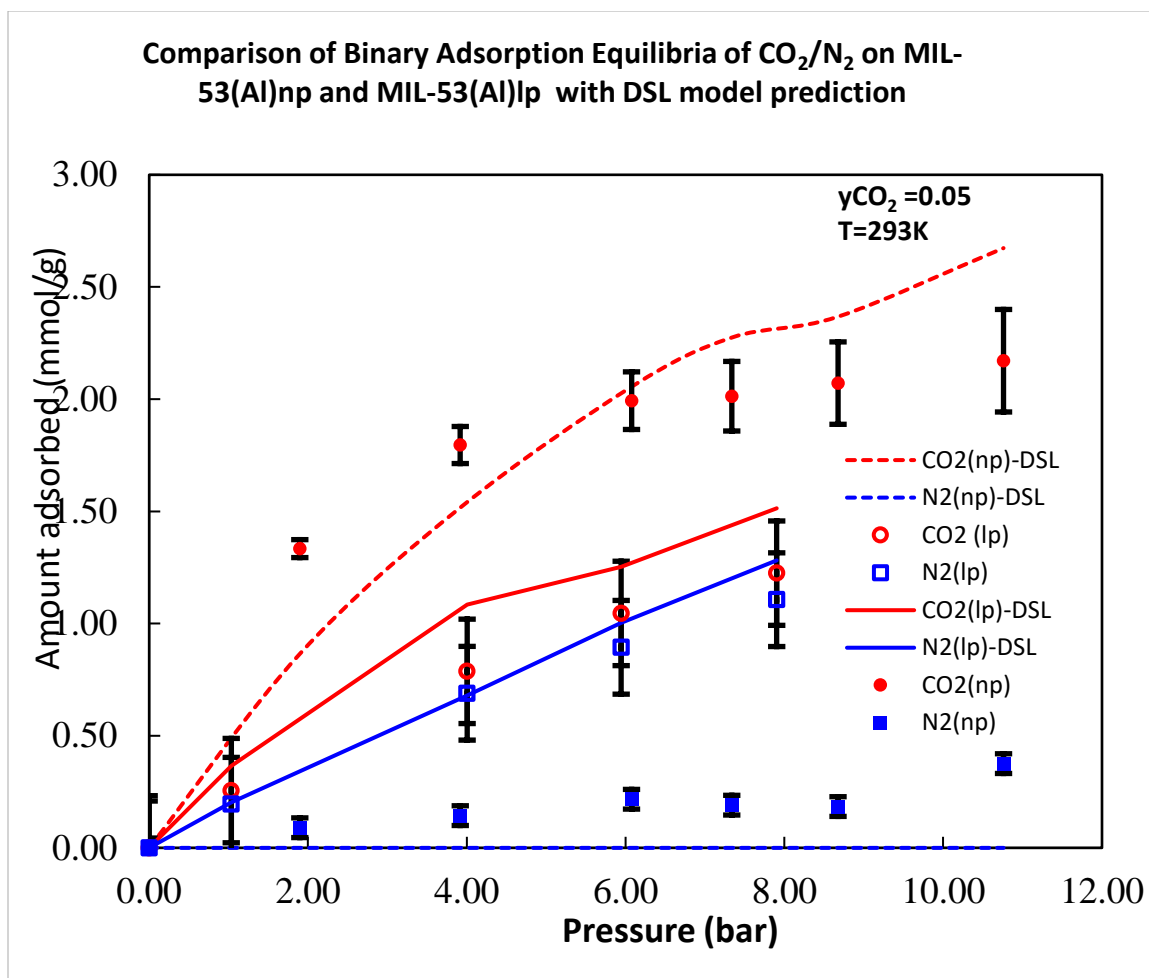


Figure 16: Difference in the binary adsorption characteristics of the np and lp phase

The above figure compares the binary adsorption equilibria of CO₂ and N₂ binary mixture on MIL-53(Al)np and MIL-53(Al)lp at constant CO₂ composition of 0.05 and constant temperature of 293 K. The results demonstrate the difference in the adsorption characteristics of the narrow and large pore phase. The narrow pore phase has a higher affinity for CO₂ and lower affinity for N₂ at this condition when compared with the large pore phase, resulting in MIL-53(Al)np having a better CO₂ selectivity for the separation of the CO₂/N₂ binary mixture.

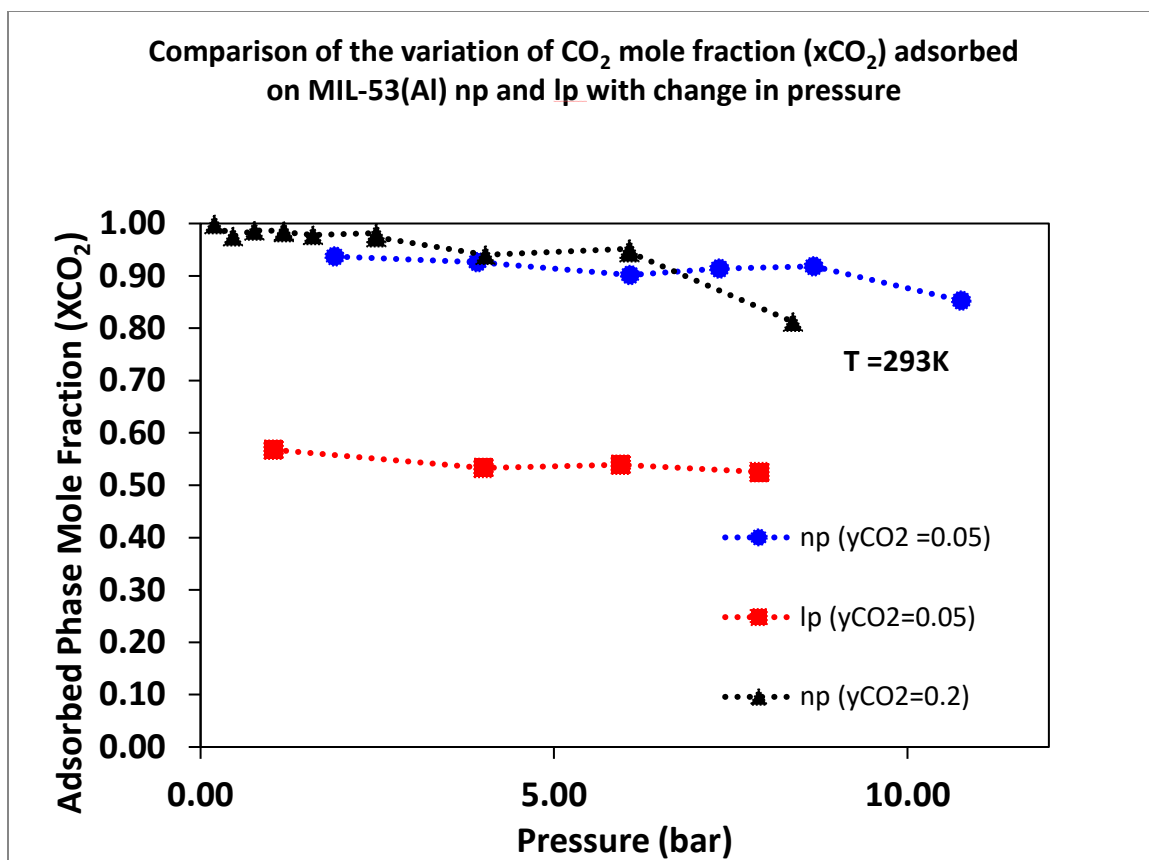


Figure 17: Effect of pressure on Adsorbed phase mole fraction

A plot of the CO₂ mole fraction in the adsorbed phase while varying the pressure is shown Figure 17 above. The experiments were conducted under constant CO₂ conditions of 0.05 and 0.2 for MIL-53(Al)np and 0.05 for MIL-53(Al)lp. All experiments were conducted at a constant temperature of 293 K. The CO₂ mole fraction remains approximately constant with change in pressure for the above stated conditions. However, the CO₂ mole fraction on the adsorbed phase of MIL-53(Al)np is significantly higher than that of MIL-53(Al)lp. These observations suggest that MIL-53(Al) CO₂ affinity is dependent on its phase not dependent on pressure.

The average mole fraction of CO₂ on the adsorbed phase of MIL-53(Al)np at CO₂ gas phase composition of 0.05 was 0.92 and 0.99 at CO₂ gas phase composition of 0.2. In

contrast, the CO₂ mole fraction of the adsorbed phase of MIL-53(Al)lp at CO₂ gas phase composition of 0.05 was 0.52. The results illustrate the dependence of the amount of CO₂ adsorbed on the phase of the material and the CO₂ gas phase composition.

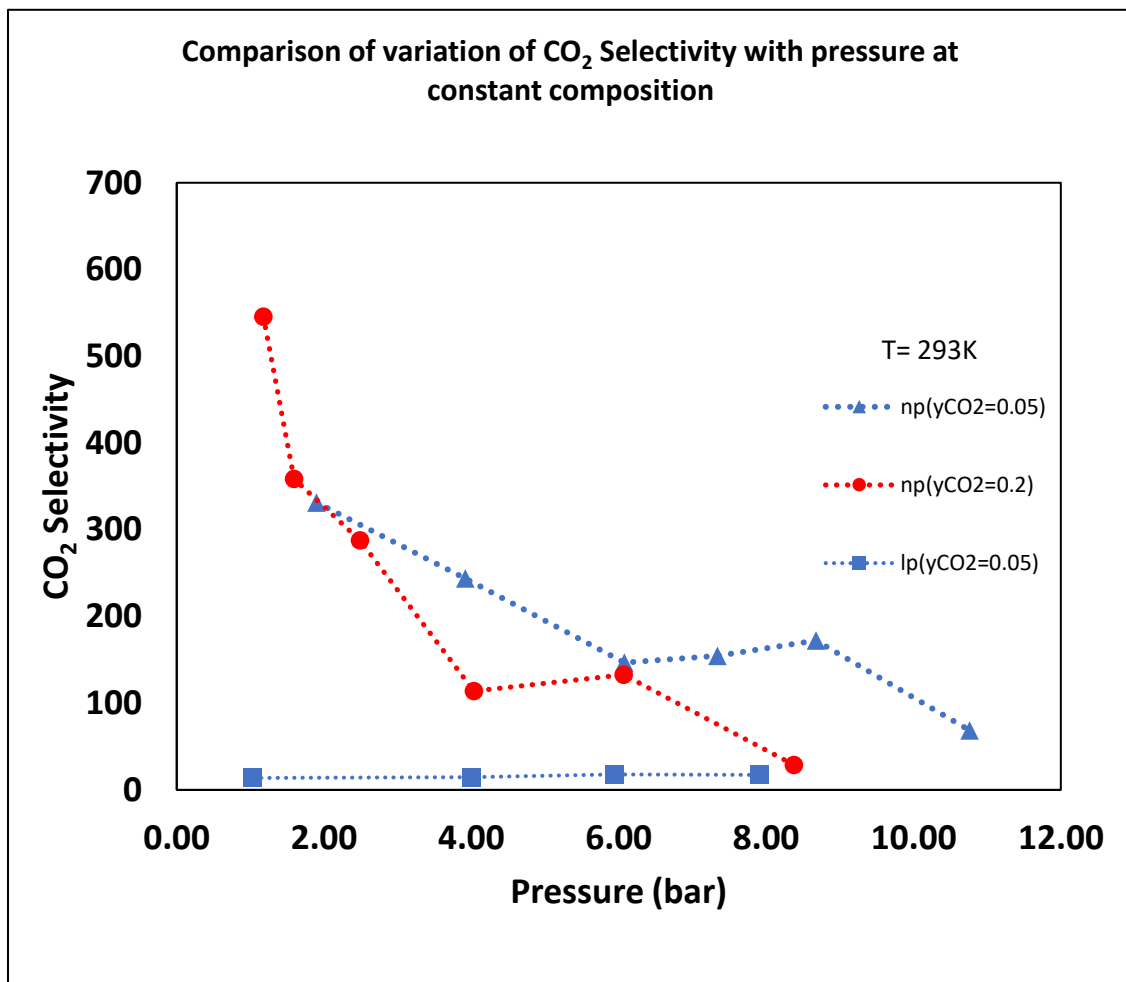


Figure 18: Effect of pressure on the selectivity of the np and lp phase of MIL-53(Al)

The variation of the selectivity of MIL-53(Al)np and MIL-53(Al)lp with pressure are shown in Figure 18. The selectivity of MIL-53(Al)np is seen to decrease with an increase in pressure for MIL-53(Al) np while the selectivity of the large pore phase remains relatively constant with pressure change. For MIL-53(Al) np there exist a

region where the selectivity remains relative constant. This lies between 4-6 bar for CO₂ composition of 0.2 and 6-8.7 bar for CO₂ composition of 0.05.

5.4 Binary Adsorption Equilibria Predictions

The binary adsorption equilibria were modelled using the revised dual site Langmuir (DSL) model extended to multicomponent mixtures. The underlying assumption of this modelling approach is that the phase transition of the MIL-53(Al) sample is dependent on the difference in the spreading between the large and narrow pore phase at the condition of interest as well as the initial state of the material (history). The model under predicted the CO₂ coadsorption capacity at conditions with CO₂ partial pressure in the range of 0.1-0.4 bar. In contrast, the model provided a good estimate of the N₂ coadsorption capacity at all the binary conditions investigated in this study.

CHAPTER VI

CONCLUSIONS AND RECOMMENDATIONS

6.1 Conclusions

This study focused on investigating the difference in the adsorption characteristics of both conformations of MIL-53(Al). This material is a flexible metal-organic framework that undergoes structural transition due to changes in temperature, pressure and upon the adsorption of certain guest molecules like CO₂. The difference in the adsorption characteristics of the narrow and large pore phase of MIL-53(Al) was studied by measuring and analyzing the pure and binary adsorption isotherms of CO₂ and N₂. The narrow pore phase was shown to have an increased affinity for CO₂ at sub-atmospheric pressure and a decreased affinity for N₂ when compared to the large pore phase. Consequently, the narrow pore phase displayed a very high selectivity towards CO₂ in the binary adsorption equilibria, even at very low CO₂ gas phase compositions. On the contrary, the adsorption of CO₂ and N₂ was competitive on the large pore phase at low CO₂ gas phase compositions. This result demonstrates that the narrow pore phase would be much more selective towards CO₂ in the separation of CO₂ from a CO₂/N₂ mixture when compared with the performance of the large pore phase.

The pure and binary gas adsorption equilibria were modelled based on the assumption that the transition of MIL-53(Al) between both phases is dependent on the

difference in spreading pressures and the initial state (history) of the MIL-53(Al) sample. The narrow and large pore saturation capacities were determined to be 3.5 mol/kg and 12.1 mol/kg respectively. The np-lp structural transition was determined to occur at a mean spreading pressure value of 1.7 Nm^{-1} with a standard deviation value of 0.6 (indicating the range of spreading pressure in which the transition occurs). The affinity parameter of the np phase for CO_2 was determined as 4.1 bar^{-1} . The np phase N_2 affinity parameter was determined to be negligible. In contrast, the lp phase CO_2 and N_2 affinity parameters were determined as 0.34 bar^{-1} and 0.02 bar^{-1} respectively.

6.2 Recommendations

In order to further understand the adsorptive behavior of MIL-53(Al), it is recommended that additional binary adsorption equilibria measurements should be performed at conditions intermediate between those conducted in this study (for example on the np form at ~ 4 and 10 bar).

Furthermore, synthesis techniques that control the crystal size distribution can be investigated to help understand the dependence of the transition pressure range on the MIL-53(Al) crystal size distribution.

Lastly, the pure and binary adsorption isotherms should be measured at two additional temperatures, to determine the temperature dependence of the spreading pressure.

REFERENCES

1. Yaghi, O. M., Li, H., Davis, C., Richardson, D. and Groy, T. L. Synthetic Strategies, Structure Patterns, and Emerging Properties in the Chemistry of Modular Porous Solids [†]. *Acc. Chem. Res.* **31**, 474–484 (1998).
2. Kitagawa, S. and Uemura, K. Dynamic porous properties of coordination polymers inspired by hydrogen bonds. *Chem. Soc. Rev.* **34**, 109 (2005).
3. Férey, G. and Serre, C. Large breathing effects in three-dimensional porous hybrid matter: facts, analyses, rules and consequences. *Chem. Soc. Rev.* **38**, 1380 (2009).
4. Kitagawa, S., Kitaura, R. and Noro, S. I. Functional porous coordination polymers. *Angew. Chemie - Int. Ed.* **43**, 2334–2375 (2004).
5. Fletcher, A. J., Thomas, K. M. and Rosseinsky, M. J. Flexibility in metal-organic framework materials: Impact on sorption properties. *J. Solid State Chem.* **178**, 2491–2510 (2005).
6. Liu, Y., Her, J., Dailly, A. and Ramirez-cuesta, A. J. Reversible Structural Transition in MIL-53 with Large. 11813–11818 (2008).
7. Li, J.-R., Kuppler, R. J. and Zhou, H.-C. Selective gas adsorption and separation in metal–organic frameworks. *Chem. Soc. Rev.* **38**, 1477 (2009).
8. Mellot-Draznieks, C., Serre, C., Surblé, S., Audebrand, N. and Férey, G. Very large swelling in hybrid frameworks: A combined computational and powder diffraction study. *J. Am. Chem. Soc.* **127**, 16273–16278 (2005).
9. Millange, F., Serre, C., Férey, G. Synthesis, structure determination and properties of MIL-53as and MIL-53ht: the first Cr^{III} hybrid inorganic -organic microporous solids: Cr^{III}(OH).{O₂C-C₆H₄CO₂}.HO₂C-C₆H₄-CO₂H)_x. *Chem. Commun.* 822–823

(2002). doi:10.1039/b201381a

10. Serre, C., Bourrelly, S., Vimont, A., Ramshaye, N.A., Maurin, G., Llewellyn, P.L., Daturi, M., Filinchuk, Y., Leynaud, O., Barnes, P. and Ferey, G. An explanation for the very large breathing effect of a metal-organic framework during CO₂ adsorption. *Adv. Mater.* **19**, 2246–2251 (2007).
11. Loiseau, T., Serre, C., Huguenard, C., Fink, G., Taulelle, F., Henry, M., Bataille, T. and Ferey, G. A Rationale for the Large Breathing of the Porous Aluminum Terephthalate (MIL-53) Upon Hydration. *Chem. - A Eur. J.* **10**, 1373–1382 (2004).
12. Smith, J. M., Van Ness, H. C. and Abbott, M. M. *Introduction to Chemical Engineering Thermodynamics. Chemical Engineering* **27**, (2005).
13. Lowell, S., Shields, J. E., Thomas, M. A. and Thommes, M. *Characterization of Porous Solids and Powders: Surface Area, Pore Size and Density. Springer Netherlands* **16**, (2004).
14. Deng, S. Sorbent Technology. *Encycl. Chem. Process.* 2825–2845 (2006).
doi:10.1081/E-ECHP-120007963
15. Zhou, H.-C., Long, J. R. and Yaghi, O. M. Introduction to Metal–Organic Frameworks. *Chem. Rev.* **112**, 673–674 (2012).
16. Li, J. R., Ma, Y., McCarthy, M.C., Sculley, J., Yu, J., Jeong, H., Balbuena, P.B. and Zhou, H. Carbon dioxide capture-related gas adsorption and separation in metal-organic frameworks. *Coord. Chem. Rev.* **255**, 1791–1823 (2011).
17. Sumida, K., Rogow, D.L., Mason, J.A., McDonald, T.M., Bloch, E.D., Herm, Z.R., Bae, T. and Long, J.R. Carbon dioxide capture in metal-organic frameworks. *Chem. Rev.* **112**, 724–781 (2012).

18. Li, J., Cheng, S., Zhao, Q., Long, P. and Dong, J. Synthesis and hydrogen-storage behavior of metal-organic framework MOF-5. *Int. J. Hydrogen Energy* **34**, 1377–1382 (2009).
19. Wu, H., Gong, Q., Olson, D. H. and Li, J. Commensurate adsorption of hydrocarbons and alcohols in microporous metal organic frameworks. *Chem. Rev.* **112**, 836–868 (2012).
20. Li, J. R., Sculley, J. and Zhou, H. C. Metal-organic frameworks for separations. *Chem. Rev.* **112**, 869–932 (2012).
21. Stock, N. and Biswas, S. Synthesis of metal-organic frameworks (MOFs): Routes to various MOF topologies, morphologies, and composites. *Chem. Rev.* **112**, 933–969 (2012).
22. Rocha, J., Carlos, L. D., Paz, F. A. A. and Ananias, D. Luminescent multifunctional lanthanides-based metal–organic frameworks. *Chem. Soc. Rev.* **40**, 926–940 (2011).
23. Hardy, S. W., February, R., Journal, M. and Chemistry, P. The Expansion of Charcoal on Sorption of Carbon Dioxide. **15**, (1927).
24. Fuchs, A. H. and Cheetham, A. K. Adsorption of guest molecules in zeolitic materials: Computational aspects. *J. Phys. Chem. B* **105**, 7375–7383 (2001).
25. Boutin, A., Coudert, F.X., Spring-Huet, M.A., Neimark, A.V., Férey, G. and Fuchs, A.H. The behavior of flexible MIL-53(Al) upon CH₄ and CO₂ adsorption. *J. Phys. Chem. C* **114**, 22237–22244 (2010).
26. Férey, G., Serre, C., Devic, T., Maurin, G., Jobic, H., Llewellyn, P.L., Weireld, G.D., Vimont, A., Daturi, M. and Chang, J. Why hybrid porous solids capture

- greenhouse gases? *Chem. Soc. Rev.* **40**, 550–562 (2011).
27. Horcajada, P., Surble, S. Serre, C., Hong, D., Seo, Y., Chang, J., Greneche, J., Margiolaki, I. and Ferey, G. Synthesis and catalytic properties of MIL-100(Fe), an iron(III) carboxylate with large pores. *Chem. Commun.* **100**, 2820–2822 (2007).
 28. Bourrelly, S., Llewellyn, P. L., Serre, C., Millange, F. and Loiseau, T. Different Adsorption Behaviors of Methane and Carbon Dioxide in the Isotypic Nanoporous Metal Terephthalates MIL-53 and MIL-47. 13519–13521 (2005).
doi:10.1021/ja054668v
 29. William, M. P. and Walton, K. S. Journal of Colloid and Interface Science Effect of synthesis solvent on the breathing behavior of MIL-53 (Al). *J. Colloid Interface Sci.* **447**, 33–39 (2015).
 30. Bourrelly, S., Llwellyn, P.L., serre, G., Millange, F., Loiseau, T. and Ferey, G. Different Adsorption Behaviors of Methane and Carbon Dioxide in the Isotypic Nanoporous Metal Terephthalates MIL-53 and MIL-47. doi:10.1021/ja054668v
 31. Finsy, V., Ma, L., Alaerts, L., De Vos, D.E., Baron, G.V. and Denayer, J.F.M. Microporous and Mesoporous Materials Separation of CO₂ / CH₄ mixtures with the MIL-53 (Al) metal – organic framework. *Microporous Mesoporous Mater.* **120**, 221–227 (2009).
 32. Neimark, A. V, Coudert, F. X., Boutin, A. and Fuchs, A. H. Stress-based model for the breathing of metal-organic frameworks. *J. Phys. Chem. Lett.* **1**, 445–449 (2010).
 33. Ortiz, A. U., Springuel-Huet, M. A., Coudert, F. X., Fuchs, A. H. and Boutin, A. Predicting mixture coadsorption in soft porous crystals: Experimental and

- theoretical study of CO₂/CH₄ in MIL-53(Al). *Langmuir* **28**, 494–498 (2012).
34. Coudert, F., Jeffroy, M., Fuchs, A. H., Boutin, A. and Mellot-draznieks, C. Thermodynamics of Guest-Induced Structural Transitions in Hybrid Organic # Inorganic Frameworks Thermodynamics of Guest-Induced Structural Transitions in Hybrid Organic-Inorganic Frameworks. 14294–14302 (2008).
doi:10.1021/ja805129c
35. Mishra, P., Edubilli, S., Uppara, H. P., Mandal, B. and Gumma, S. Effect of Adsorbent History on Adsorption Characteristics of MIL- 53 (Al) Metal Organic Framework. **53**, (2013).
36. Llewellyn, P. L., Maurin, G., Devic, T., Loere-serna, S., Rosenbach, N., Serre, C., Bourelly, S., Horcajada, P. Fillinchuk, Y. and Ferey, G. Prediction of the conditions for breathing of metal organic framework materials using a combination of X-ray powder diffraction, microcalorimetry, and molecular simulation. **130**, 12808–12814 (2008).
37. Mishra, P., Uppara, H. P., Mandal, B. and Gumma, S. Adsorption and Separation of Carbon Dioxide Using MIL-53(Al) Metal-Organic Framework. *Ind. Eng. Chem. Res.* **53**, 19747–19753 (2014).
38. Edubilli, S. History Dependent Model for Pure Gas Adsorption on MIL-53(Al). Unpublished work, IIT Guwahati, India (2018)
39. Coudert, F.X. The osmotic framework adsorbed solution theory: predicting mixture coadsorption in flexible nanoporous materials. *Phys. Chem. Chem. Phys.* **12**, 10904 (2010)
40. Myers, A. L. and Monson, P. A. Physical Adsorption of Gases: the Case for

Absolute Adsorption as the Basis for Thermodynamic Analysis. 1–52

41. Tykodi, R. J. Thermodynamics of adsorption. *J. Chem. Phys.* **22**, 1647–1654 (1954).

APPENDIX A

Propagation of error analysis in primary measurements

Estimating the impact of uncertainties in experimental measurements on thermodynamic properties is necessary as some of the quantities measured depend on accuracy of the measurement of others. The pure and binary component adsorption experimental data was collected using closed volumetric system. The measurements involved in the closed system that appear in equations used to calculate total and partial amounts adsorbed are:

- Pressure measured by a transducer at different times.
- Volumes that are measured in the different parts of the apparatus using helium expansion techniques.
- Temperature measured by a thermocouple in the column and controlled by an external bath.
- Gas composition at equilibrium measured using gas chromatograph (GC) and
- Mass of porous solid in the column which was measured using balance.

Indeed, all these measurements are related to only three measurements:

i.) Pressure, ii.) Mass, and iii.) Temperature.

There are numerous ways to estimate the uncertainties in measurements that have impact on final calculated results. One technique used in the present work is propagation of error analysis, which calculates the most probable errors on the final results. If a quantity N is calculated by a mathematical expression,

$$N = f(P, T) \qquad \qquad \qquad A. 1$$

Where the uncertainty in the measurement of P and T are ΔP and ΔT respectively,
the uncertainty in N i.e. ΔN can be calculated as follows

$$\Delta N = \left(\left(\left(\frac{\partial P}{\partial N} \right) * \Delta P \right)^2 + \left(\left(\frac{\partial T}{\partial N} \right) * \Delta T \right)^2 \right)^{0.5} \quad \text{A. 2}$$

APPENDIX B

Pure Component Adsorption Equilibria Data on MIL-53(Al) at 293 K

In this section the experimental data of the pure component adsorption isotherms of CO₂ and N₂ on MIL-53(Al) shown in Figure 6 and are presented

Table B. 1: Pure CO₂ experimental isotherm data on MIL-53(Al) at 293 K

Pressure(bar)	N(mmol/g)	Standard error (\pm)
0.05	0.12	0.001
0.17	0.42	0.002
0.27	1.05	0.004
0.38	1.70	0.006
0.47	2.03	0.008
0.65	2.35	0.011
0.92	2.57	0.014
1.15	2.72	0.019
1.50	2.90	0.024
2.40	3.23	0.034
3.07	3.41	0.047
3.78	3.55	0.061
4.65	3.74	0.077
4.96	4.42	0.092
5.21	5.24	0.106
5.54	6.28	0.121
5.93	7.13	0.135
6.34	7.68	0.150
6.72	8.14	0.165
6.97	8.34	0.179
7.21	8.54	0.194
7.86	8.84	0.210
8.75	9.11	0.228
9.54	9.30	0.248
10.00	9.39	0.268
10.48	9.48	0.289
10.86	9.55	0.309

Table B. 2 Pure CO₂ experimental isotherm data on MII-53(Al)np at 293 K

Pressure(bar)	N(mmol/g)	Standard error (\pm)
0.02	0.19	0.00
0.04	0.50	0.00
0.05	0.84	0.00
0.10	1.31	0.00
0.21	1.83	0.00
0.28	2.03	0.00
0.37	2.17	0.01
0.45	2.27	0.01
0.53	2.37	0.01
0.66	2.46	0.01
0.79	2.55	0.01
0.87	2.60	0.02
1.15	2.74	0.02
1.31	2.81	0.02
1.64	2.93	0.03
1.96	3.03	0.04
2.40	3.23	0.034
3.07	3.41	0.047
3.78	3.55	0.061
4.65	3.74	0.077
4.96	4.42	0.092
5.21	5.24	0.106
5.54	6.28	0.121
5.93	7.13	0.135
6.34	7.68	0.150
6.72	8.14	0.165
6.97	8.34	0.179
7.21	8.54	0.194
7.86	8.84	0.210
8.75	9.11	0.228
9.54	9.30	0.248
10.00	9.39	0.268
10.48	9.48	0.289
10.86	9.55	0.309

Table B. 3 Pure N₂ experimental isotherm data on MIL-53(Al)_{lp} at 293 K

Pressure(bar)	N(mmol/g)	Standard error (±)
0.19	0.04	0.00
0.38	0.09	0.00
0.53	0.12	0.01
0.68	0.16	0.01
0.85	0.20	0.01
1.02	0.22	0.02
1.46	0.32	0.02
1.74	0.37	0.03
2.22	0.48	0.04
2.63	0.56	0.05
2.91	0.66	0.05
3.90	0.86	0.07
4.65	1.01	0.08
5.03	1.08	0.10
5.75	1.21	0.11
6.46	1.34	0.13
6.84	1.41	0.15
7.76	1.57	0.17
8.75	1.71	0.19
9.59	1.85	0.21
10.93	2.06	0.24
11.84	2.20	0.27
12.40	2.29	0.30

Table B. 4 Pure N₂ experimental isotherm data on MIL-53(Al)lp at 293 K

Pressure(bar)	N(mmol/g)	Standard error (\pm)
0.75	0.01	0.01
0.88	0.01	0.01
2.02	0.03	0.02
3.02	0.06	0.04
4.10	0.11	0.06
5.00	0.21	0.08
6.09	0.34	0.10
7.08	0.60	0.12
7.91	0.98	0.15
11.22	1.88	0.19
12.86	2.10	0.23

APPENDIX C

Binary Adsorption Equilibria Data on MIL-53(Al) at 293 K

In this section the experimental data of the binary adsorption isotherms of CO₂ and N₂ mixture on MIL-53(Al)np are presented

Table C. 1 Binary Adsorption equilibria experimental data on MIL-53(Al)np at 0.8 bar

CO ₂ mole fraction(y_{CO_2})	N (mmol g ⁻¹) (CO ₂)	Standard error (±)	N (mmol g ⁻¹) (N ₂)	Standard error (±)
0.05	0.50	0.017	0.00	0.017
0.06	1.14	0.016	0.01	0.016
0.20	1.80	0.017	0.01	0.017
0.39	2.11	0.017	0.01	0.017
0.60	2.30	0.026	0.00	0.026
0.80	2.43	0.035	0.00	0.034
0.94	2.50	0.042	0.00	0.041

Table C. 2 Binary Adsorption equilibria experimental data on MIL-53(Al)np at 1.3 bar

CO ₂ mole fraction(y_{CO_2})	N (mmol g ⁻¹) (CO ₂)	Standard error (±)	N (mmol g ⁻¹) (N ₂)	Standard error (±)
0.04	0.97	0.025	0.06	0.024
0.09	1.47	0.024	0.05	0.024
0.21	1.97	0.026	0.03	0.026
0.43	2.32	0.029	0.01	0.029
0.51	2.44	0.037	0.00	0.036
0.52	2.45	0.036	0.00	0.036
0.61	2.55	0.043	0.00	0.042
0.61	2.54	0.043	0.00	0.043
0.79	2.67	0.056	0.00	0.056
0.79	2.66	0.055	0.00	0.055
0.88	2.72	0.065	0.00	0.064
0.88	2.71	0.063	0.00	0.063
0.93	2.75	0.069	0.00	0.068

Table C. 3 Binary Adsorption equilibria experimental data on MIL-53(Al)np at 9.5 bar

CO ₂ mole fraction(y_{CO_2})	N (mmol g ⁻¹) (CO ₂)	Standard error (±)	N (mmol g ⁻¹) (N ₂)	Standard error (±)
0.05	1.31	0.198	1.27	0.192
0.10	2.47	0.218	0.82	0.210
0.12	2.55	0.199	1.00	0.192
0.22	3.60	0.206	1.01	0.197
0.37	5.48	0.212	0.55	0.202
0.55	7.31	0.294	0.60	0.279
0.76	8.47	0.391	0.22	0.368
0.88	9.47	0.458	0.20	0.428
0.93	9.65	0.503	0.03	0.469

Table C. 4 Binary Adsorption equilibria experimental data on MIL-53(Al)np at 0.20 y_{CO_2}

Pressure	N (mmol g ⁻¹) (CO ₂)	Standard error (±)	N (mmol g ⁻¹) (N ₂)	Standard error (±)
0.20	0.51	0.004	0.00	0.004
0.46	1.35	0.010	0.02	0.010
0.76	1.65	0.016	0.01	0.016
1.18	1.93	0.025	0.01	0.025
1.18	1.93	0.025	0.02	0.025
1.59	2.11	0.034	0.02	0.033
2.49	2.31	0.052	0.02	0.052
2.49	2.30	0.052	0.03	0.052
4.03	2.48	0.085	0.08	0.084
6.07	2.70	0.129	0.07	0.126
6.07	2.69	0.129	0.08	0.126
8.38	2.49	0.179	0.29	0.173

Table C. 5 Binary Adsorption equilibria experimental data on MIL-53(Al)np at 0.05 y_{CO_2}

Pressure	N (mmol g ⁻¹) (CO ₂)	Standard error (±)	N (mmol g ⁻¹) (N ₂)	Standard error (±)
1.90	1.33	0.040	0.09	0.040
3.92	1.80	0.083	0.14	0.081
6.07	1.99	0.128	0.22	0.126
7.34	2.01	0.155	0.19	0.151
8.68	2.07	0.184	0.18	0.178
10.76	2.17	0.228	0.38	0.220

Table C. 6 Binary Adsorption equilibria experimental data on MIL-53(Al)lp at 0.05 y_{CO_2}

Pressure	N (mmol g ⁻¹) (CO ₂)	Standard error (±)	N (mmol g ⁻¹) (N ₂)	Standard error (±)
1.03	0.26	0.022	0.19	0.022
4.00	0.79	0.085	0.69	0.083
5.94	1.04	0.126	0.89	0.123
7.90	1.22	0.167	1.11	0.163